4-24-2019

Predicting Weather-Caused Power Outages: Technique Development, Evaluation, Applications

Diego Cerrai
University of Connecticut - Storrs, diego.cerrai@uconn.edu

Predicting Weather-Caused Power Outages: Technique Development, Evaluation, Applications

Diego Cerrai, Ph.D.

University of Connecticut, 2019

Storms are the primary cause of extensive power outages in electric distribution networks. Storm power outage prediction is therefore fundamental for an efficient and effective response to weather-based power outages. In this work, we address the problem of storm outage prediction by improving an existing outage prediction model (OPM) originally developed for thunderstorm and extratropical storms, and extending its structure for predicting outages associated with mixed phase precipitation (snow, ice, freezing rain) events. The herein developed OPMs use either regression trees or statistical models fed by numerical weather prediction outputs, leaf area index (LAI), infrastructure, land cover, soil type, elevation, and historical outage data to forecast number and spatial distribution of power outages during storms. OPM improvements for thunderstorms and extratropical storms consist in the introduction of new modules: a storm classifier, a multimodel optimization, and a module for implementing LAI. Cross-validation results show that the median absolute percentage error of the new OPM decreases from 130 percent to 59 percent for outage predictions at the service territory level, and that the OPM skills for operational forecasts are consistent with the skills based on historical storm analyses. Beyond thunderstorms and extratropical storms OPMs, two models are developed for predicting power outages during snow and ice storms: a machine learning (ML) based model predicting outages on a regular 4-km grid, and a generalized linear model (GLM) for power outage prediction at the town level. The most important variables for both models are assets, leaves on trees, snow density, and - for the ice model only - freezing rain and gusts. Coss-validation results

show that the GLM has more skills than ML models for extreme events prediction, while ML models have better performance for lower impact events and present lower errors in the spatial distribution. The creation of reliable OPMs also allowed us to quantify the effects of a resiliency improvement on the power grid (the Enhanced Tree Trimming, ETT), using two independent methodologies. The first approach is a statistical study of the change of frequency of outage-free locations. The second approach uses the OPM as a vulnerability assessment tool to evaluate the change in the number of outages before and after ETT. From the statistical approach we show a 49% to 65% reduction of the outage-free grid cells during thunderstorms and extratropical storms coming from tree trimming. The OPM based analysis indicated that storm outages were reduced between 16% and 48% after performing ETT.

Predicting Weather-Caused Power Outages: Technique Development, Evaluation, Applications

Diego Cerrai

B. Physics, University of Pisa, 2012

M. Physics of the Earth System, University of Bologna, 2015

A dissertation

Submitted in Partial Fulfillment of the

Requirements for the Degree of

Doctor of Philosophy

At the

University of Connecticut

2019

APPROVAL PAGE

Doctor of Philosophy Dissertation

Predicting Weather-Caused Power Outages: Technique Development, Evaluation, Applications

Presented by

Diego Cerrai, B.S., M.S.

Major Advisor _____
Emmanouil Anagnostou

Associate Advisor _____
Marina Astitha

Associate Advisor _____
Malaquias Peña

Associate Advisor _____
Guiling Wang

Associate Advisor _____
David Wanik

University of Connecticut

2019

Acknowledgements:

I wouldn't have been here without my former advisor, Prof. Vincenzo Levizzani. He introduced me to high-level scientifiic research and he suggested me to come to the University of Connecticut where I found the best environment to grow. Here, Prof. Emmanouil Anagnostou, an exceptional person at work and outside, allowed me to give the best of myself in research and obtain better and better results.

I would like to thank my mother, Cecilia, my father, Paolo, and my sister, Chiara. They always supported me, even in the hard and heartbreaking choice to leave my country. I would like to thank my beautiful husband, Daniele (*just married!*), who, despite the distance, has always been next to me day and night. Now we are finally under the same roof, and our love, support and care for each other is ever-increasing. Thanks also to the rest of my amazing family.

Thanks to my best friend Matteo, always present anywhere and anytime, and to Simone, Gaja, Isaac, Alessandro, friends with whom I spend unforgettable moments. Thanks to Paolo, Dario and to all my other friends from my hometown, Livorno.

Thanks to my friends from the University of Pisa and the University of Bologna, now living around the world, and also to Stefano, Anna, and to the other italian friends that I found here in Connecticut.

Finally, to my current and former labmates Ehsan, Marika, Feifei, Peter, Guannan, Berk, Dave and Xinxuan, I owe you my thanks for always supporting me and allowing me to obtain the best results, and my excuses, for contacting you at night, before the impact of storms, to run more simulations, to fix small issues in the operational system, or simply to help providing better results.

Contents

Chapter 1

Executive summary

Predicting the impact of storms on electric distribution networks is a very challenging task, because interactions between weather, vegetation and infrastructure are non-linear and chaotic. Historically, utility managers have been predicting power outages by combining the information of weather predictions with their knowledge of the electric power system. However, subjective predictions and evaluations of possible impacts have been difficult to defend in public hearings after the impact of severe storms. More recently, new statistical and machine learning techniques have opened the way to the aggregation of multiple weather, vegetation, infrastructure and land cover inputs for spatially distributed outage prediction.

In Connecticut, in the early 2010s, it started to be evident that a system based only on managers' intuition was not an optimal way to manage storm preparedness. The damaging consequences of prolonged power outages had been extensively experienced by the Connecticut population in 2011 and 2012, when two hurricanes (Sandy and Irene) and a strong noreaster (2011 Halloween noreaster) hit the State. After the impact of the first two storms, a Two Storm

Panel was formed by Governor Malloy to review the *prevention, planning and mitigation of impacts associated with emergencies and natural disasters that can reasonably be anticipated* [2]. A recommendation of the Two Storm Panel was the development of a collaboration between the State, utilities and a university to *develop a more robust hazard assessment capability that can identify 'hot spots' for storm damage and integrate early warning with preparedness and emergency management* [2]. This and other recommendations expressed in the report were taken up by the Eversource Energy Center (EEC) at the University of Connecticut, a center of excellence for the study of the mitigation of the risks affecting the electric grid, and that is sponsoring the work presented in this dissertation.

Studying and advancing the predictability of weather related power outages has therefore become a major component of storm preparedness. In the Northeastern United States most power outages are caused by disruption of overhead lines from tree branches due to severe weather events [3]. The amount of these disruptions depends on meteorological and environmental factors that can be quantified and modeled, despite the theory of deterministic chaos [4] suggesting that we will never be able to predict in advance the exact number of storm outages.

This work aims at understanding the interactions between overhead lines, vegetation and weather phenomena, through the improvement of an existing outage prediction model (OPM) and the development of new outage prediction models, to forecast the number and spatial distribution of power outages in advance of upcoming storms. The importance of storm-caused outage predictions lies in the fact that the knowledge of the expected storm damages allows electric utilities emergency managers effectively allocate crews and resources. Crews in particular may be requested to other out-of-state utilities when an impactful

storm is approaching a territory. For a timely emergency response in such situations, the driving time of the crews has to be taken into consideration, and the outage prediction has to be communicated to the emergency managers with a lead-time that depends on the severity of the storm's impact.

This research discussed in this dissertation has three main objectives:

- Predict storm outages through new representations of weather and vegetation;
- Develop outage prediction models for snow and ice storms;
- Assess the effects of a vegetation management standard on the rate of outages in a distribution grid.

Each objective will be thoroughly investigated in the next three chapters. Chapter 2 is focused on the improvements of an existing OPM [5],[6] for thunderstorms and extratropical storms prediction in Connecticut. Model advancements consist in the introduction of three new modules: (i) a storm classifier based on weather variables, (ii) a multimodel optimization of regression tree output and (iii) a post-processing routine for more accurately describing tree-leaf conditions. Improvements are demonstrated through leave-one-storm-out cross-validations performed on 76 extratropical storms and 44 thunderstorms. A comparison between model predictions using forecasts and analysis is also performed.

In chapter 3, two new models for predicting mixed phase precipitation events (blizzards, ice storms, freezing rain) are developed. The first, based on decision tree models, allows to predict the number of power outages on a 4-km grid. The second, based on a generalized linear model, is a model for outage prediction at the town level. Both models are cross-validated in multiple configurations, and their variable importance is evaluated, for understanding what are the most

relevant parameters for the models.

In chapter 4, the impact of a vegetation management standard on the rate of outages is evaluated through two different approaches. A statistical study of the change of outage-free location frequency due to tree trimming is compared to an evaluation of the change of number of outages due to tree trimming, by using the OPM developed in chapter 2 as a vulnerability assessment tool. Results of the assessment will be presented and discussed separately for 100 extratropical storms and for 44 thunderstorms.

Chapter 2

Predicting Storm Outages through New Representations of Weather and Vegetation [1]

2.1 Introduction

Electricity is a foundation of modern society [7], [8], and unreliable electric power delivery has direct and long-term socio-economic effects [9], [10]. Predicting the variability of electricity usage, in the form of forecasting the balance between energy production [11], [12], [13], demand [14], [15], [16], [17], and outages [18], [19], is essential for addressing the reliability of power delivery.

An important reliability component is weather-based outages. Storms can cause severe disruption in the electric grid, affecting human activities [20], secu-

rity and life [21], [22]. Advancing the predictive understanding of the relationships between weather and power outages is a key step for creating a resilient electric grid, capable of withstanding the current increase of weather-caused power outages [23] and the expected increase in severe weather events [24].

In the Northeastern United States, major power outages can be caused by singular failures on the transmission system that serves hundreds of thousands of customers [25]. In contrast, most daily outages are produced by tree branches falling on overhead distribution lines [3], that typically serve tens to hundreds of customers. During storms, power outages occurrence is determined by a complex interaction among atmospheric phenomena, vegetation cover, and infrastructure. Accurate storm power outage predictions and early communication of predicted impacts to the utilities in the face of this complexity are necessary for efficient emergency preparedness, support and response [26].

The first attempt to develop an outage prediction model can be found in [18], where a negative binomial regression model [27] was used to evaluate the relative importance of transformers, wind speed, and random effects during three hurricanes. In the decade that followed, several studies on outage prediction modeling were conducted. [28] used Generalized Linear Models (GLMs, [27]) to investigate the importance of hurricane and ice storm variables for outage prediction, and to improve the previous formulation of the [18]'s hurricane outage prediction model. Advances were obtained with a better variable selection [29], with the use of Generalized Additive Models (GAMs, [30]) for hurricane outage predictions [31], and with the implementation of a random forest (RF, [32]) model [33]. The usefulness of a hybrid classification tree/regression method for handling the zero-inflation was discussed in [34], while [35] used classification and regression trees (CARTs, [36]) for demonstrating that some land cover variables are proxies for the power system, hence useful for predicting outages.

Building on [33], the Spatially Generalized Hurricane Outage Prediction Model (SGHOPM, [37]) combined elevation, land cover, soil and vegetation with the wind characteristics included in the first version [38], to improve prediction skill. More recently, [39] used also vegetation management and tree height data derived from LiDAR for enhancing outage prediction accuracy by identifying the vegetation at risk for striking overhead lines.

By exploiting the knowledge derived from previous studies, this paper builds upon a comprehensive Outage Prediction Model (OPM), presented in [5] (hereafter, W15) and [6] (hereafter, H17). The model was developed for predicting outages associated with the main types of weather events affecting the Northeastern United States, including thunderstorms, snow storms, extratropical and tropical cyclones, by using state-of-the-art meteorological, statistical, and machine learning (ML) techniques. The OPM presented in W15 and H17 and its improvements have been used since 2015 to issue forecasts for Eversource Energy-Connecticut and since early 2017 for Massachusetts and New Hampshire service territories.

Previous studies on the OPM have highlighted different aspects of outage prediction. In particular, from the evaluation of eight ML techniques conducted in W15, an ensemble (ENS) model consisting of predictions from a decision tree (DT, [36]), a RF and a boosted tree (BT, [40]) model, that used weather hindcasts (dynamical downscaling of weather analyses), infrastructure and land cover data as inputs, emerged as spatially better performing than each individual model. In H17, a comparison between a Bayesian additive regression trees (BART, [41]) model and a quantile regression forest (QRF, [32], [42]) model yielded "inconsistent performances of both models for varying season categories (tree-leaf condition) implying difficulties in predicting storm outages with leaves on trees". This study also determined that the BART model surpassed QRF in

predicting the total number of outages over the entire service territory.

Although both studies used variables extracted from weather hindcasts as inputs to the outage models, neither evaluated operational or pseudo-operational performances computed on actual weather forecasts, after the outage models were built. It is well known, however, that even within a short range of days (one to two), weather forecasts can be associated with significant error [43], due to uncertainties in initial conditions - see Lorenz [4] for a theoretical approach and [44] for a case study over the East Coast - and limitations in physical parameterizations of unresolved physics, such as the cumulus [45] or planetary boundary layer schemes [46]. Therefore, performance evaluation based on weather hindcasts, despite its wide use in outage prediction literature, is not sufficient for describing the overall performance of an outage forecasting model.

In this study we aim at addressing the main challenges identified in previous works, by introducing and describing the implementation of three new modules into the OPM: 1) a *storm classifier* to allow different ML model calibrations for meteorologically distinct storm types and quantify uncertainties for each type; 2) a *leaf area index (LAI)* parameter determined from satellite data to account for dynamic leaf conditions that affects the relationship among various weather parameters (wind gust, snow, ice) and power outages; and 3) an *optimization* that combines ML model outputs based on training error characteristics, to reduce outage modeling error. We conduct cross-validations in different model configurations based on 12 years of historical events (120 storms) with the intent to demonstrate improvements brought about by the new modules. To evaluate actual operational performance, we also compare OPM skills for one year of analyzed events (25 storms) with the skills of OPM driven by weather forecasts initialized 24 hours before the selected events.

2.2 The Outage Prediction Framework

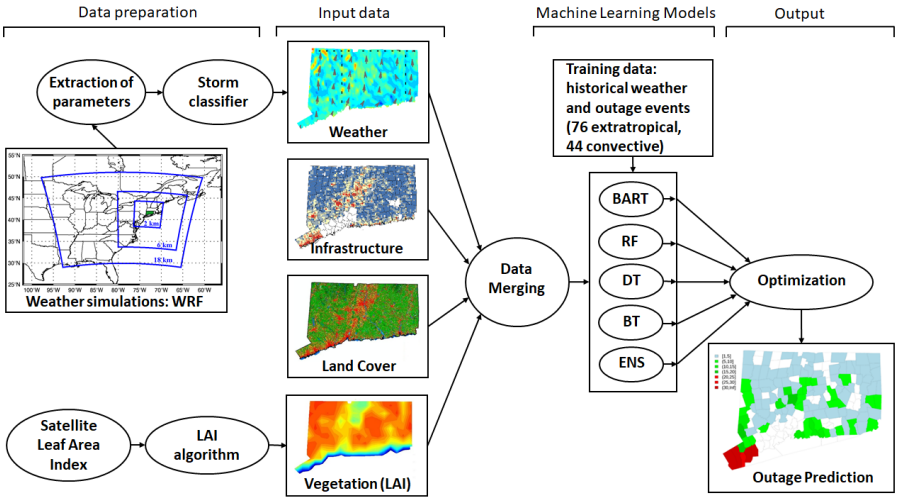

Figure 2.1: Outage prediction model architecture.

The OPM is an operational forecasting framework that integrates weather predictions with infrastructure, land cover and vegetation characteristics to predict, through the use of machine learning models, distributed storm power outages across utility service territories in the Northeastern United States (Figure 2.1). This section aims at describing the OPM structure.

2.2.1 Input data

The OPM inputs are listed in Table 2.1, and derive from different sources: weather data (groups b,c,d,e) generated from numerical weather prediction (NWP) model; land cover (coniferous, deciduous and developed area) and vegetation (LAI) variables retrieved from satellites; and infrastructure data describing assets in the overhead distribution network provided by the distribution company. These input datasets have been chosen because forest and land cover type, along with the amount of leaves on trees in a given period of the year

strongly influence how weather phenomena interact with overhead lines, causing power outages.

Variable	Description	Group	Units
PercConif	Percentage of coniferous forest	a	%
PercDecid	Percentage of deciduous forest	a	%
PercDevel	Percentage of developed area	a	%
Wgt5	Duration of wind at 10 m above 5 m/s	b	hr
Wgt9	Duration of wind at 10 m above 9 m/s	b	hr
Wgt13	Duration of wind at 10 m above 13 m/s	b	hr
MaxW10m	Maximum wind at 10 m	b	m s^{-1}
Cowgt5	Continuous duration of wind at 10 m above 5 m/s	b	hr
Cowgt9	Continuous duration of wind at 10 m above 9 m/s	b	hr
Cowgt13	Continuous duration of wind at 10 m above 13 m/s	b	hr
MeanW10m	Mean wind at 10 m	b	m s^{-1}
Ggt13	Duration of wind gusts at 10 m above 13 m/s	c	hr
Ggt17	Duration of wind gusts at 10 m above 17 m/s	c	hr
MaxGust	Maximum wind gusts at 10 m	c	hr
MeanGust	Mean wind gusts at 10 m	c	m s^{-1}
MaxTotPrec	Total precipitation	d	mm
MaxPreRate	Maximum precipitation rate	d	mm h^{-1}
MeanPreRate	Mean precipitation rate	d	mm h^{-1}
MaxSoilMst	Maximum Soil Moisture	e	m^3 m^{-3}
MeanSoilMst	Mean Soil Moisture	e	m^3 m^{-3}
MaxSpHum	Maximum Specific Humidity	e	g g^{-1}
MaxTemp	Maximum Temperature	e	K
MeanTemp	Mean Temperature	e	K
LAI	Leaf area index	f	m^2 m^{-2}

Table 2.1: Description of the predictor variables used in the OPM.

Such data are rescaled and matched on a common grid, to constitute the "storm analysis", a summary of measured or predicted conditions for each storm. A detailed description of the sources of each input variable, of the data preparation, and of the process that allows to rescale and match the data on a common grid is provided in the next paragraphs. The reasons behind the classification of the variables into six different groups are described in Section 2.3.

Weather

For each storm, weather data are computed at 2 km grid spacing through the Weather Research and Forecasting (Advanced Research WRF-ARW, v.3.7.1 [47], [48]) NWP model. The WRF produces high-resolution weather forecasts (future conditions) and hindcasts (past conditions) by dynamcally downscaling Global Forecast System (GFS) data, used as inital and boundary conditions. GFS data are produced by the National Center for Environmental Prediction (NCEP) and are available at six-hourly intervals on a 0.25 degree grid. Weather forecasts and hindcasts are created by applying a two-way nesting technique on three nested domains. This technique allows to remove numerical noise at the boundaries between different domains, through interactive inter-domain communication [49], [50], [51].

We fixed an outer domain covering most of the Eastern United States with 18 km grid spacing; a 6 km intermediate domain capturing the Northeastern United States, and an inner domain at 2 km grid spacing, centered over Connecticut, providing the final high-resolution forecast for the study area. The WRF model is set up with the configuration described by Table 2.2. WRF operational forecasts are updated daily at http://cee-wrf.engr.uconn.edu/.

Parametrization	**Scheme**
Microphysics	New Thompson et al. [52]
Cumulus	Grell 3D Ensemble Scheme [53] [54]
Planetary Boundary Layer	Yonsei University [55]
Surface Layer	MM5 Similarity [56], [57], [58], [59] [60]
Land Surface Model	Unified Noah [61]
Longwave Radiation	RRTM [62]
Shortwave Radiation	Goddard RRTMG [63] [64]

Table 2.2: Parametrization schemes used in the WRF Model.

Weather simulations are processed by extracting new parameters summarizing wind, precipitation and soil data over the entire storm life (48 hours for extratropical and 36 hours for convective storms) for each grid cell:

- Maximum value (MaxW10m, MaxGust, MaxSoilMst, MaxSpHum, MaxTemp, MaxTotPrec, MaxPreRate): maximum value of any selected variable;
- Mean value (MeanW10m, MeanGust, MeanPreRate, MeanSoilMst, MeanTemp): mean value of any selected variable computed in the 4-hour window of highest mean 10m wind;
- Occurrence value (Wgt5, Wgt9, Wgt13, Ggt9, Ggt17): number of hours of wind speed or wind gusts above given thresholds over the specified storm duration;
- Continuous duration value (Cowgt5, Cowgt9, Cowgt13): maximum continuous duration (in hours) of sustained winds above a certain threshold.

Wind- and gust-related variables are used because the primary stress on trees during most of the storms is caused by winds. Precipitation changes the resistance of the wood, adds weight to tree (particularly in the form of snow or ice), and increases soil moisture, contributing to loosen the bonds between roots and soil, which may cause uprooting.Specific humidity and temperature depict additional stress on trees and infrastructure. Moreover, given that the majority of the outages occur during the storm peak, a characterization of both the peak intensity and of the duration of adverse meteorological conditions during an event are used in our model.

Storms are subsequently classified (through the classification introduced in Section 2.2.4) according to their dominant meteorological characteristics. This allows to select different relevant input variables for different storm types, for facilitating the learning tasks of the machine learning models.

Infrastructure

Utility infrastructure data were provided by Eversource Energy and reported as geolocated protective devices. Such data are proprietary and owned by the utility company. We aggregated infrastructure data at the 2 km grid cells used by the WRF model, in order to create a variable, *sum of assets*, representing the total number of electric transformers, fuses, reclosers, and switches in each grid cell.

Land cover

The land cover dataset was created by the University of Connecticut Center for Land Use Education and Research (CLEAR) at 30 m resolution [65]. Data were aggregated into 2 km grid cells by considering the land cover in the immediate proximity (60 m) of overhead lines, following W15.

Vegetation

Vegetation characteristics are present in the model through the LAI, a dimensionless quantity that measures the green leaf area per unit ground surface area [66]. The original dataset is available from the NASA Earth Observations (NEO) project [67], which is part of the NASA Earth Observing System project [68]. It is derived from the Moderate Resolution Imaging Spectroradiometer (MODIS) aboard the Terra and Aqua satellites, which acquires images at 500 meters resolution, and is scaled and resampled at 0.1° spatial and eight-day temporal resolutions. The dataset is available for the 2000-2016 time period, and an algorithm that we developed for this study (Section 2.2.4) allows to process, quality control and rescale the entire dataset at the 2 km grid.

2.2.2 Response Variable: Historical Outage Data

The number of electric power outages per 2 km grid cell per storm represents the response variable of the OPM. Outages are defined as locations where at minimum a two-man restoration crew is needed for manual intervention to restore power (W15, H17). Historical, geolocated power outages recorded by the Eversource Outage Management System (OMS) were aggregated on the 2 km grid by storm. We identified the storm dataset using an outage intensity and a weather severity approach: (i) we computed the 95^{th} percentile of the daily outage distribution on the Eversource service territory, and, in agreement with utility managers, defined storm days as the days that exceeded this percentile; (ii) we applied the storm classifier (introduced in Section 2.2.4) to the Automated Surface Observing System (ASOS) airport station data, to include the storms with significant weather, but whose outages were not in the top 5^{th} percentile. Based on these approaches we identified 76 extratropical storms and 44 convective storms, which were simulated using the WRF model, and we aggregated such data with the other input data for the OPM to create a storm analysis dataset. The total service territory outages per storm in the database range between 24 and 3,590 for extratropical storms, and between 92 and 1,042 for thunderstorms or convective events, following a log-normal distribution of outages for the territory and a general negative binomial distribution at town and grid cell level totals (not shown). Most outages occurred over densely populated Southwestern Connecticut (Figure 2.2a and 2.2b).

For having an overview of the most vulnerable areas, we removed the dependence of outages on infrastructure (Figure 2.2c and 2.2d). Specifically, we normalized the outages occurring in each town by the sum of the assets in that territory, and we found differences in the impact between extratropical and convective storms. Since many extratropical storms lie over the ocean, major

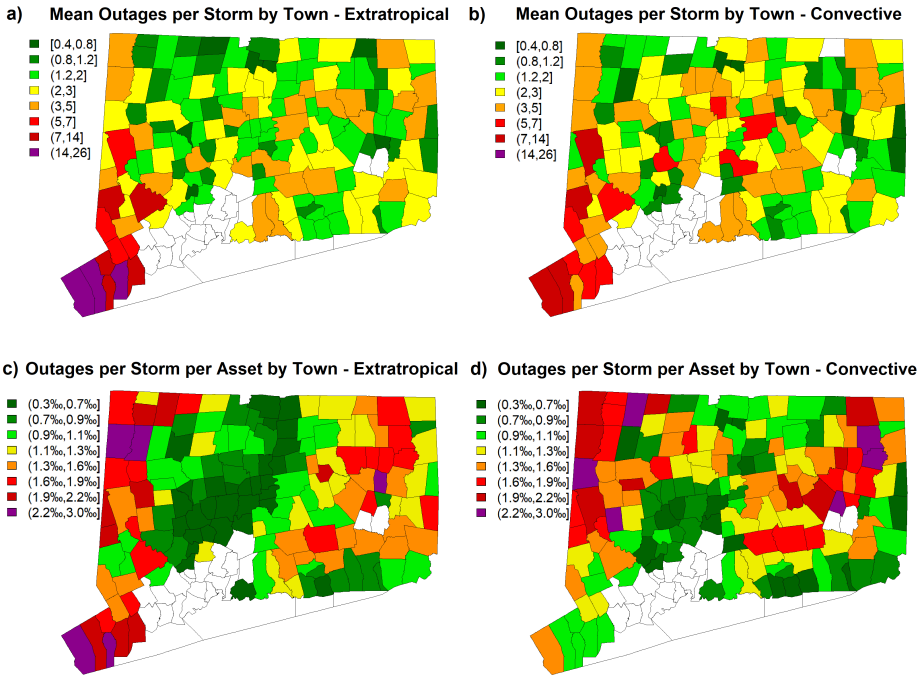

Figure 2.2: Mean storm outages by town for: a) extratropical, b) convective storms. Mean outages per storm per assets by town for c) extratropical, d) convective storms.

outages were concentrated across the coastal area, mainly in the southwestern coastal region (with more than two outages per thousand assets in an average extratropical storm) and in high-elevation areas in northeastern Connecticut (Figure 2.2c). The impact of convective storms, in contrast, was inland (Figure 2.2d), especially in the highly vegetated areas of northeastern and northwestern Connecticut. Despite this statistical information on the average storm impact is not used by the OPM, it provides a descriptive overview of the spatial characteristics of the interactions between infrastructure and different storm types.

2.2.3 Machine Learning Models

For training the nonparametric models used in the OPM, we used historical storm analyses, composed of a summary of weather hindcasts, land cover, LAI, electric utility assets and historical outages for a range of storms with substantial impact within Connecticut. The models allow to predict the number of future (using weather forecasts) or past (using weather hindcasts) power outages during a storm, at the same 2 km grid used for the input variables.

To limit the effect of correlated predictors, input data were preprocessed by performing a principal component analysis (PCA, [69], [70]) using a varimax rotation [71], and by keeping the first 10 components, that explained between 85% and 95% of the model variability in our datasets. The machine learning models used in the OPM are the following:

- Decision Tree (DT): a series of decision nodes ('if-then' statements) that, starting from a 'root node', allows to recursively split the training data into subsets of similar values for the response variable (outages) [72]. In this work we use the CART [36] method, that allows a generation of only two "branches" from each decision node. Dataset partitioning occurs through the minimization of the sum of square error (SSE).

- Gradient Boosted Tree (BT) [40]: a model that fits small decision trees "weak lerners" on the residuals of decision trees of fixed size "base learners". The residuals are the deviations of the observed values from the mean value of each partition. Since the trees fitted on the residuals may lead to overfitting, a learning rate is used to reduce the corrections obtained by such trees. Similar to W15, one thousand trees were fitted, with a learning rate of 0.1.

- Random Forest (RF) [32]: a collection of decision trees trained on a ran-

dom subset of training data, using a random subset of predictors. Similarly to W15, two hundred trees were created for our random forest model.

- Ensemble regression (ENS): a decision tree model trained on the DT, BT and RF outputs to refine their predictions. The ENS attempts to find new patterns in the ML outputs, which may yield better results than any single model. The DT, BT and RF outputs are the only three variables that are inputted into a final decision tree model (ENS). This model was previously found to have better spatial accuracy than individual ML models in W15.

- Bayesian Additive Regression Tree (BART) [41]: it is a sum of regression tree models:

$$Y = \sum_{j=1}^{m} g_j(x, T_j, M_j) + \epsilon. \tag{2.1}$$

where $g_j(x; T_j, M_j)$ is the contribution provided to the model by the j^{th} regression tree; x is the vector of predictors; T_j and M_j are respectively the set of tree nodes and of terminal nodes for the j^{th} tree; and ϵ is the variance component, assumed to be $N(0, \sigma^2)$. We set a number of trees $m = 30$, and starting from prior specifications for T_j, M_j and σ, we used ten thousand iterations in the Markov Chain Monte Carlo (MCMC [73]) algorithm to reach convergence. Once convergence was reached, we used four thousand iterations to obtain the predictions. A similar configuration was used in H17.

Model outputs, in the form of outage predictions, are either aggregated at the town level and presented as power outage maps, or aggregated at the distribution company level, and presented as total outages on the territory. Since discrepancies in the predictions were found among the different ML models, in the new OPM version, the predictions of the five models are post-processed

through a statistical optimization (Section 2.2.4). After the final outage predictions are generated, they are communicated to emergency response personnel, who use this information to develop preparedness measures for facing the incoming storm and to increase the resilience of the affected territories through more accurate planning and an estimation of the time to restoration [74], [75].

2.2.4 New Modules

Three new modules have been added to the OPM framework and are presented in this work: the LAI was added to take into account of the interactions between power lines and vegetation; the storm classifier was introduced to allow the ML models to be calibrated with different variables for different storm types; and an optimization technique was implemented for improving OPM results based on past performance of the different ML models.

Leaf Area Index

Following the recommendations of H17, we created an algorithm for implementing a quality controlled LAI information in the OPM (Figure 2.3). The LAI variable allows to consider the variability of power outage occurrence created by the varying amount of leaves that are on the trees. The algorithm was necessary because the original NEO dataset contained a substantial amount of missing data, primarily due to clouds and interpolation effects, and its use was indicated for basic analysis or trend detection.

The first step of the LAI data processing algorithm was the formulation, for each eight-day period, of a first guess at the climatological LAI values and anomalies for the region of interest. The missing data present in the original dataset were not considered in the computation of climatological values. The second step consisted in the estimation of the missing values by using the tem-

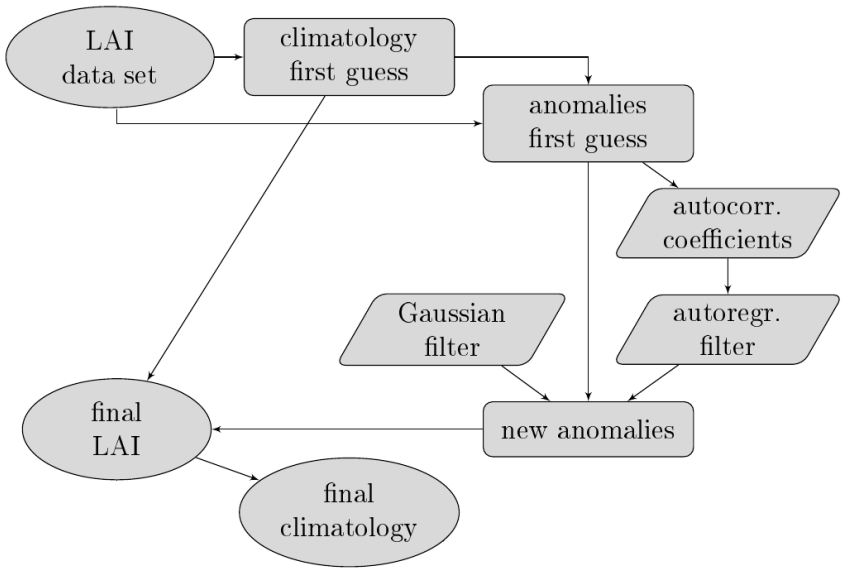

Figure 2.3: Algorithm for LAI data processing and correction.

poral autocorrelation function of the first guess climate anomalies (departures from the first guess climatology) of the dataset. We found the LAI values, at any point, to be (weakly) correlated at a 0.05 significance level with the LAI values measured in the previous eight-day period; but no significant correlation occurred for a distance of two or more time steps. We estimated the anomaly for each missing point, by using a combination of an autoregressive model of order 1 -AR(1), by considering both previous and successive values - and a Gaussian filter on the valid data. The new anomalies were added to the first guess of the climatology to compute the corrected LAI values, whose missing data were compensated for because in locations for which the LAI could not be retrieved using neighboring values, the value of the first guess at the climatology was used. From this new LAI dataset we computed the new eight-day climatological values of LAI that are used in the OPM, as well as the new anomalies.

Storm Classifier

Weather prediction accuracy as well as the interactions among weather parameters, vegetation and infrastructure, vary for distinct storm types. In order to consider the different errors occurring in both meteorological analysis and forecasts for different types of weather, and to allow the models to use only the variables that successfully describe the processes involved for each type, we introduced a storm classification, grouping events to extratropical and thunderstorms. In future model developments we will also introduce hurricanes/tropical system and snow/ice events.

Following [76] and [77], the storms hitting the considered territory were classified into four different categories, according to the dominant meteorological conditions and to the scale of the processes involved:

- Convective storms at the mesoscale: events of short duration (minutes to a few hours) characterized by lightning, high rain rate, strong wind gusts, and, in some cases, hail. These thunderstorms may either be embedded in a frontal system (in any season) or isolated and created by diurnal heating of the surface (usually in summer and late spring).

- Extratropical storms at the synoptic scale: extratropical storms exhibiting heavy rain and winds and lasting from several hours to a few days. Such events in our database are most frequent during the fall.

- Snow and ice storms: events characterized by wintry precipitation, such as snow, sleet, and freezing rain, and often associated with strong winds.

- Hurricanes: tropical cyclones characterized by long duration of strong sustained winds and wind gusts, and high precipitation rates.

We created an algorithm for retrospectively classifying all the storms in the

database using surface meteorological observations and forecasts valid 24 hours prior to the storm start time. The algorithm used the following criteria:

- If the storm produced one or several tornadoes (identified by the National Weather Service), the event was not included in any data set, because the short-range weather hindcasts and the forecasts analyzed lacked tornado predictability.

- If the storm was classified as a "hurricane" or "tropical storm" by the National Hurricane Center, we applied the same classification in the OPM. Two hurricanes have hit New England in the last 10 years: Irene (August 2011) and Sandy (October 2012). They were extensively studied in W15 and in [19].

- If the storm produced a water equivalent of at least 5 mm of wintry precipitation over at least 25 percent of the territory, we classified it as a snow or ice storm. Wintry precipitation was not included in this study.

- If wind gusts of at least 13 m/s lasting less than five consecutive hours associated with precipitation of at least 10 mm in one hour were measured or predicted, or if the event was officially reported as "thunderstorm" at at least one airport station, and if gusts exceeding 13 m/s for more than five hours were not measured or predicted at all the other airport stations, we classified the storm as convective at the mesoscale. We classified 44 thunderstorms with these characteristics into this category.

- If the above conditions were not satisfied, and wind gust exceeding 17 m/s were measured or predicted in any location, we classified the storm as extratropical at the synoptic scale. We selected 76 extratropical storms for this study.

This algorithm was not only used for classifying historical storms, but is also operationally used for triggering the OPM. The algorithm replaces the storm categorization algorithm based on the time of the year, introduced in W15 and H17. In that algorithm the absence of information on the condition of tree leaves was partially compensated for by the categorization into "cold season" (having little or no leaf coverage), "warm season" (having high leaf coverage) and "transition period" (having intermediate leaf coverage). However, despite the occurrence of predominant processes across different seasons climatologically reflects the storm type categorization, different storm types can occur in each season, which limits the ability of seasonal categorization to capture the unique storm characteristics.

The foundation of the storm classification was based on the fact that different variables are important for different storm types for physical (predominant processes) and model structure (weather model inaccuracy) reasons. While it could be argued that the inclusion of all weather model output variables in the OPM could lead to better performance, empirical evidence (Section 2.4.1) demonstrates that spurious interactions may lead to overfitting.

Optimization

We introduced a module for optimally combining the ML model predictions and providing the best estimate of the outage prediction, by taking into account historical model performances. The outage prediction F_k for the k^{th} storm was obtained as a linear combination of the five non-parametric models predictions ($p_{i,k}$):

$$F_k = \sum_{i=1}^{5} c_{i,k} \cdot p_{i,k} \tag{2.2}$$

The coefficients $c_{i,k}$'s were computed by maximizing an objective function

with the characteristics of robustness for different orders of magnitude and of absence of overweightness of some statistics with respect to others. The oversensitivity to very damaging storms rendered inadequate the results produced by the least squares minimization, hence we introduced the ratio U between the mean absolute percentage error (MAPE) and the Nash-Sutcliffe coefficient (NSE, [78]):

$$U = \frac{NSE}{MAPE} \tag{2.3}$$

where the NSE (defined in Appendix A.1) is a nondimensional measure of efficiency, ranging between $-\infty$ and 1, that determines the magnitude of the residual variance of a regression analysis relative to the initial, observed variance; and the MAPE is defined in Appendix A.1. The estimation of the coefficients $c_{i,k}$ for each storm is performed by considering only the remaining storms. Such coefficients are used for predicting outages related to the excluded storm.

The function U allowed us to simultaneously optimize two of the statistics (NSE, MAPE) indicated as most important by [79], while taking into account the main characteristic of the dataset: that the storm total outages follow a strongly right-skewed log-normal distribution (not shown). For this reason the overfitting toward strong events obtained by the maximization of the NSE was balanced by the high weight given to the many low impact events, which was obtained with the denominator of the function.

2.3 Methodology

This section describes the methodology used for demonstrating outage prediction skills improvements brought about by the new modules implemented into the OPM for the Eversource Connecticut service territory.

2.3.1 Cross-Validation

We used the historical storm dataset described in Section 2.2.2 to conduct leave-one-(storm)-out-cross-validations (LOOCV, [80], [81], [82]) experiments in presence and absence of the implemented modules.

The LOOCV at the storm level consists in predicting outages of any storm by calibrating a model using all the storms present in the historical dataset except for the considered storm. We chose this method because both the k-fold cross-validation and the repeated random holdout validation - e.g. [83] for a complete overview - used in W15 and H17, respectively, do not reflect the scope needed in an outage prediction model - that is, the ability to forecast damages from a storm whose outages are originally unknown at any location. Both k-fold and repeated randomized holdout may use strongly correlated neighboring data for the storm of interest in the model calibration. In a LOOCV framework, on the other hand, the knowledge of weather-related outages in neighboring areas from the same storm cannot be used. Moreover, results obtained using a LOOCV are directly comparable with operational model settings, with the unique difference that a storm forecast is used in place of the analysis.

2.3.2 Experimental setup

The LOOCV experiments on the storm dataset were organized as follows:

i) We tested the skills of the five machine learning models (BART, ENS, RF, DT, and BT) in the same configuration used in W15 and H17 (with a seasonal categorization).

ii) We implemented the optimization module and created the OPT model. We quantified the improvements brought about by the optimization by comparing the OPT skills with the skills of each ML model.

iii) We additionally implemented the the LAI module and created the OPT_LAI

model. We compared the OPT model skills with the OPT_LAI ones.

iv) For testing the importance of the implementation of the storm classifier, we designed 20 LOOCV experiments (Table 2.3), that allowed us to evaluate the sensitivity of the model to different categories of input variables (Table 2.1). In category *(a), land cover and assets*, we included static variables related to infrastructure and land cover. In groups *(b), wind, (c), gust, and (d), precipitation*, we included all the variables outputted from the weather model or computed during a post-processing that were, respectively wind-, gust-, or precipitation-related. In group *(e), near-surface*, we included the remaining important weather variables computed below the ground or at the surface. Finally, for demonstrating the improvements from adding the vegetation annual variability, we created category *(f), leaves*, with LAI as its unique variable. The only group common to all sensitivity experiments was *(a), land cover*, since W15 demonstrated that the variables in this category were significant for the OPM. Experiments 11-20 corresponded to 1-10, with the addition of *(f), leaves*. Each odd-numbered experiment differed from the even-numbered one after it in that *(c), gusts*, were added to the latter. Experiments 1-8 and 11-18 inclued *(b), wind*, while 9, 10, 19, and 20 did not. Experiment 18 was the most complex, containing all the predictors listed in Table 2.1.

v) We then selected the two best performing models (one with and another without LAI) for each storm class, and compared their skills with the OPT model skills, that used a seasonal categorization.

vi) We also computed the aggregated (extratropical and convective) skills of the new model that has all the implementations (OPT_LAI_CLA) and compared with the skill of both the OPT_LAI model and of the OPT_CLA model, selected from experiments 1-10.

Experiment	Group	Experiment	Group
1	a, b	11	a, b, f
2	a, b, c	12	a, b, c, f
3	a, b, d	13	a, b, d, f
4	a, b, c, d	14	a, b, c, d, f
5	a, b, e	15	a, b, e, f
6	a, b, c, e	16	a, b, c, e, f
7	a, b, d, e	17	a, b, d, e, f
8	a, b, c, d, e	18	a, b, c, d, e, f
9	a, d, e	19	a, d, e, f
10	a, c, d, e	20	a, c, d, e, f

Table 2.3: Sensitivity tests.

2.3.3 Verification Metrics

We computed the error metrics described in Appendix A.1 for evaluating model skills, and the *percent improvement* (PI) for comparing changes in an error metric M between different model versions, namely 1 and 2:

$$PI = \begin{cases} 100 \cdot \frac{M_2 - M_1}{M_1} & \text{if higher values of M correspond} \\ & \text{to better performances} \\ & \\ 100 \cdot \frac{M_1 - M_2}{M_1} & \text{if lower values of M correspond} \\ & \text{to better performances} \end{cases} \tag{2.4}$$

We used the Taylor [84] diagram for evaluating model performances. The Taylor diagram uses the relationship among NCRMSE, NSD, and r to plot these three statistics in a standardized quadrant.

Since outage data are spread over different orders of magnitude, however, "correlation-based measures are inappropriate and should not be used to evaluate the goodness-of-fit of model simulation" [79], because these measures are likely to be sensitive to extreme values. [79] also recommend reporting "the observed and modeled means and standard deviations, as well as MAE or RMSE

(and probably both)", despite indicating the coefficient of efficiency as the most appropriate measure. For this reason, we chose to present and compare several statistics to find the best overall model.

In evaluating the significance of the results, it was not possible to apply common statistical techniques for error evaluation. In fact, the strong non-linearities in the model did not allow the error to be Gaussian. Hence, we considered five different pairs of cross-validations performed with the same input data and model setting. In comparisons within the pairs, each cross-validation was found not to differ more than 3% from each other on any error metric. For this reason, despite the limits imposed by the long computational time on the number of experiments we could perform, we assumed a difference of less than 3 percent between two statistics as representative of similar results while considering a greater difference as different.

2.4 Results and Discussion

In this section we present the results obtained by progressively implementing and evaluating each new module into the OPM. Results were rigorously validated using sensitivity tests in a LOOCV framework on the historical storm events. The new OPM version, obtained after implementation of all the new modules, was further evaluated in an operational framework, using the weather forecasts available the day before each storm. This last step was necessary because many decisions on the crews needed for restoration are taken one day before each storm, since this is the tradeoff between weather forecast accuracy and adequate preparedness. However, the possible presence of errors in the short-term forecasts makes performance evaluation using the weather hindcasts alone inadequate for describing the operational performance.

2.4.1 Sensitivity tests

The original, operational OPM version, described in W15 and H17, was composed of five different ML models that generated separate outage forecasts. We evaluated these models on the 120 storms that are the object of this study. Results of the model evaluation showed MdAPEs between 57% (BART) and 88% (RF), MAPEs between 117% (BT) and 160% (RF), and NSE between 0.17 (DT) and 0.45 (BART) (Table 2.4, first box). The typical feature of some of these models was a remarkable overestimation of low impact events, as shown in W15 and H17, which led to very high values of MAPE.

The information produced by each ML model was optimized using the techinque described in Section 2.2.4 to create the OPT model version, that was operational between June 2016 and January 2017 (Table 2.4, second box). The combination between the different ML models in the optimization allowed the reduction of most of the very high errors (up to 10 times) for the low-impact storms, and to correct overall biases. This optimization led to a drastic decrease of the MAPE, which halved to 65%. Analyzing the performance by storm type it is possible to notice that most of its skills came from the extratropical model, since the NSE coefficient of the convective model was not significantly different than zero, despite having lower absolute percentage errors (because of the smaller range).

The addition of the LAI module to the OPT model allowed us to create the OPT_LAI model, operational between January and June 2017. Such model was characterized by a further performance improvement, estimated between 2% and 9%, with respect to the OPT model. However, since we consider two statistics as different when their values differ each other by more than 3% (section 2.3.3), it is not possible to state that the improvement brought about by LAI lead to subsantially different results for all the considered metrics.

Model	**MdAPE**	**MAPE**	**NSE**
BART	**57%**	**130%**	**0.45**
DT	-24%	-21%	-63%
BT	-9%	+10%	-39%
RF	-37%	-23%	-29%
ENS	-19%	-12%	-20%
OPT	**47%** (+18%)	**65%** (+50%)	**0.47** (+4%)
OPT_LAI	+2%	+9%	+8%

	Extratropical			Convective		
Experiment	**MdAPE**	**MAPE**	**NSE**	**MdAPE**	**MAPE**	**NSE**
OPT	**48%**	**80%**	**0.49**	**45%**	**49%**	**0.01**
11	-6%	+2%	-62%	-35%	-43%	-100%
12	+6%	-27%	-14%	-38%	-37%	-100%
13	+4%	+9%	-34%	-45%	-35%	-74%
14	-2%	-3%	+2%	-28%	-32%	-83%
15	+11%	+5%	-48%	**29%**	**46%**	**0.42**
16	+0%	-13%	-28%	+3%	-7%	-17%
17	+21%	+0%	-24%	-3%	-9%	-24%
18	**47%**	**64%**	**0.50**	+14%	-4%	-17%
19	-28%	-41%	-36%	-17%	-9%	-49%
20	-4%	-18%	-20%	-10%	-7%	-17%

Model	**MdAPE**	**MAPE**	**NSE**
OPT_LAI_CLA	**43%** (+9%)	**59%** (+9%)	**0.53** (+13%)
OPT_CLA	-2%	-2%	-9%

Table 2.4: Summary table for the cross validations who led to model improvements. Bolded values indicate the statistics, unbolded values indicate the percent improvement (PI) with respect to the respective, bolded statistic in the same box, and values in bracket indicate the PI with respect to the previous, bolded model version.

The validity of a storm classification for outage prediction purposes was demonstrated through 20 sensitivity tests, described in Table 2.3. The results of the sensitivity experiments 11-20 (with LAI) are presented in the central part of Table 2.4, from which, for brevity, we have omitted experiments 1-10 (their aggregated results are summarized at the bottom of the table in the *OPT_CLA* model). Since the table is not easily interpreted, we follow [79] in giving primary importance to the NSE. In cases of similar results, the MdAPE and MAPE complete the evaluation of the results.

In the simulations for extratropical storms, results from experiment 18 (with the inclusion of all the predictor variables) showed the best performance with a NSE of 0.50, a median absolute percentage error of 47 percent, and a mean percentage error of 64 percent. The most important variables for this experiment were: sum of assets, total precipitation, maximum and mean temperature, and mean wind gusts. It is noteworthy that model errors around or above 50 percent derive from an outage distribution spanning more than two orders of magnitude. Similar results for all the metrics were found also in experiment 14 (without near-surface variables), which did not produce any improvement to or setback for the model. Gusts were also important, as strong improvements in the NSE could be seen between each odd experiment and the following even one. Two other relevant variables were wind and precipitation; when wind was removed, the NSE decreased by 20 percent (experiment 20), and the absence of precipitation as predictor variable (experiment 16) implied a 28 percent decrease.

For thunderstorms, the results showed a different pattern. The most skillful experiment was number 15, which used neither gusts nor precipitation and whose NSE was 0.42. For this experiment the most important variables were: sum of assets, maximum specific humidity, maximum and mean temperature, and maximum soil moisture. In all the other thunderstorm simulations, the NSE assumed lower values; simulations 11-14 in particular had no skills (NSE$\leq$0.15). This means any model that did not use near-surface parameters was unable to correctly predict outages related to thunderstorms, hence only experiments 15-20 were worth investigating. In experiment 16, the addition of gusts to the best performing model produced a significant decrease in performance in the NSE and MAPE. This could be explained by overfitting in the model (due to particular, hidden features in the limited number of storms) that emerged in these results. The overfitting could be avoided by removing some predictor vari-

ables and creating a simpler model. For the same reasons, the implementation of precipitation in the model (in experiments 17 and 18) also failed to improve the performance relative to experiments 15 and 16.

These results highlight the complexity of predicting outages when thunderstorms occur. In fact, while thunderstorms are characterized by heavy precipitation and strong gusts, these variables were not important in the models due to the difficulty of predicting the exact location of the phenomena by the WRF model - hence, the *double-penalty effect* predominated. More specifically, errors were introduced by the misplacing of the typical thunderstorm features and this penalized the model twice - once for not predicting the event in the location where it occurred (miss) and once for forecasting it at the wrong location (false alarm) [85]. The double-penalty effect, derived from important errors in thunderstorm forecasts and analyses, is reflected in the creation of models overfitted on some meteorological features that have been artificially created by the weather simulations, but which did not manifest. Hence, when the model was validated in the LOOCV, the overfitting emerged as a decrease in performance. Despite these limitations, however, the thunderstorm model had lower MAPE and MdAPE with respect to the model for extratropical storms, because of the lower range of thunderstorm-related outages.

Gaining an understanding of the strengths and weaknesses of the models for different storm types allowed us to create the new OPM version (OPT_LAI_CLA), operational since June 2017. This model allows us to use the most suitable set of variables for each storm type. The combined introduction of the classification and LAI modules led to a 13% improvements in the NSE and 9% in both MdAPE and MAPE, over the OPT version. When comparing this new OPM version with the BART model, performance improvements are drastic, varying between 17% and 63%, depending on the statistics. As the Taylor diagram

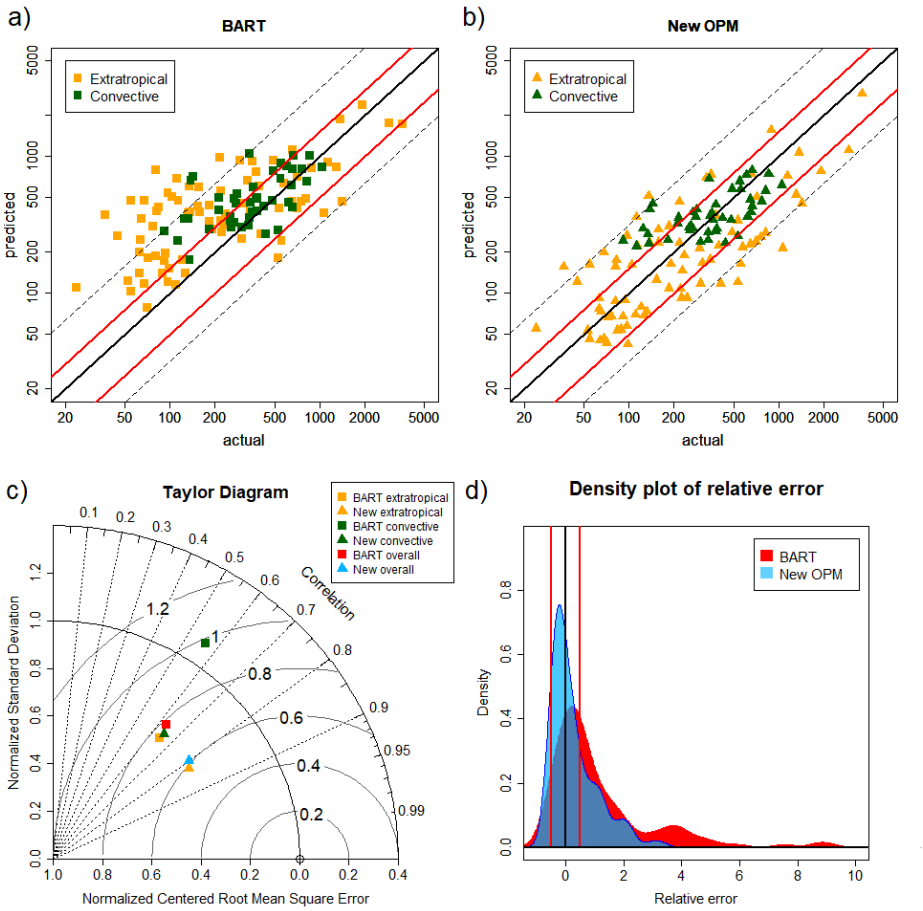

Figure 2.4: Scatter plots of predicted versus actual outages for a) the BART and b) the new OPM versions. c) Taylor diagram comparing the performances for Extratropical and Convective storms for the BART and new OPM. d) Density plot of storm total relative errors for the BART (red) and the new OPM (blue) versions. Red lines represent a 50% error, while dashed lines delimit an error of half order of magnitude.

(Figure 2.4c) shows, the NCRMSE decreased from 0.79 of the BART to 0.61 of the new OPM, and the correlation increased from 0.63 to 0.79.

Consequently, the new model allowed us to capture the order of magnitude of outages (the dashed lines in Figure 2.4a and 2.4b) for 95 percent of the storms and to predict 65 percent of the storms within a 50 percent error (thick red lines

in Figure 2.4b). This constituted a big step toward the milestone of predicting 90 percent of the events within that error and an important improvement over the 51 percent of the BART model (Figure 2.4a). From the analysis of the relative errors, it emerged that the new model has a much narrower and more centered distribution than the BART (Figure 2.4d). The main feature of the BART was the overestimation of medium and low impact events, that manifested in false alarms. The increased predictability of such events is noteworthy, since the decision-making process involves determination of the number of in- and out-of-state crews, crews travel time and associated costs, expected duration of the restoration process, and prevention from eventual penalities that utilities may face. False alarms may trigger costly prevention measures such as crews and resources allocation, and a high number of false alarms threatens the credibility of the model.

Finally, we again evaluated the importance of the LAI in the new OPM by analyzing experiments 1-10 (not shown) and summarizing the performance difference between the new OPM with LAI and without (last row of Table 2.4). After the removal of this variable, the performance decrease (between 2 percent and 9 percent) was consistent with that found for the previous model version, consolidating, but not proving, the hypothesis that the LAI is an important variable for outage prediction.

Hence, the analysis of several statistical measures of error proved that the new modules implemented in the OPM allowed drastic outage prediction improvements over each ML model introduced in W15 and H17.

2.4.2 Operational Performances

The outage prediction framework developed with the storm analyses would be a mere numerical exercise if a consistency between weather hindcasts and fore-

casts (that is, the absence of a significant bias) did not hold. To evaluate the hypothesis of consistency between outages predicted using storm forecasts and those predicted using storm analysis, we considered the events that occurred in 2016. From the comparison of the outage predictions using forecasts and analyses, shown in Figure 2.5a, it emerged that the median absolute percentage difference among each couple of forecast-analysis (18 percent) was much smaller than the MdAPE of the forecasts and of the analyses versus the actual outages (30% in both cases, Figure 2.5b and 2.5c).

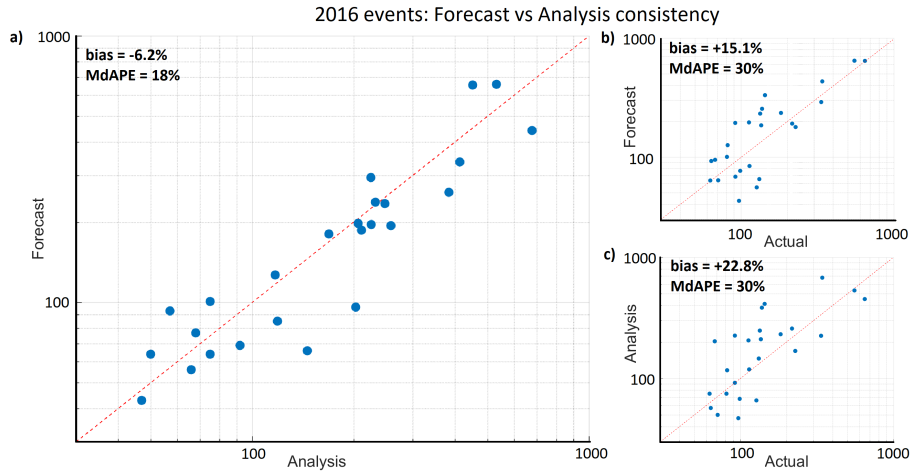

Figure 2.5: Plot of storm total outage predictions using storm forecasts versus outage predictions using analyses for storms that occurred in Connecticut during 2016 (a); plots of outage predictions using storm forecasts (b) and analyses (c) versus actual outages, for the same storms of (a).

Hence, the errors deriving from the weather model uncertainties between forecasts and analyses were a small part of the total OPM error. The major contribution to the error came from consistent inaccuracies of the weather model and from the statistical models. The biases for the 2016 storms for forecasts and analyses with respect to the actual data are 15 and 23 percent, respectively. The fact that these values are much higher than the bias between forecasts and

analyses (-6.2 percent) strengthens the finding of consistency. Furthermore, the positive values can be explained with the outage model underdispersion, which produces overestimation for medium-to-low impact events.

2.5 Conclusions

This study presented three new modules that were implemented in an existing outage prediction model and evaluated the new model predictions and improvements based on 76 extratropical and 44 convective storms. The optimization module introduced hereby led to a version that significantly outperformed each of the five machine learning models comprising the OPM. Further improvements - the addition of the leaf area index and the weather classification with a consequent variable selection - allowed the new OPM to perform with a Nash-Sutcliffe efficiency coefficient of 0.53 and to predict most of the events with a service-territory-total-outages maximum error of 43 percent. Extratropical storms, associated with a more extended historical dataset, exhibited a higher Nash-Sutcliffe coefficient than convective storms, but also a higher median absolute percentage error, because of the much wider range of outages.

We also presented operational OPM performance using the weather forecasts for a subset of the analyzed events and compared it with performance using weather hindcasts. Comparison at the service territory level showed that the high correlation and low bias between the predicted outages in the two configurations exhibited the validity of the current operational framework, which consists of calibrating the model using weather hindcasts and predicting outages using consistent weather forecasts. Errors in both forecasts and analyses can be attributed to a random component, as the misplacing of weather phenomena or to a systematic component dependet on orography, infrastructure resilience measureas and other local conditions.

We suggest further improvements for addresing the double-penalty effect, which played an important role in the random component for the thunderstorm model: these are the application of a spatial translation and matching of the forecast and observed fields [86]; the neighborhood method for upscaling the fields [87], [88], [89], or a combination of the two. The upscaling would imply an evaluation of the outage prediction obtained by aggregating the predictors at different resolutions to find the best resolution for each storm type.

Future steps also include the exploration of probabilistic outage forecasts, based on ensemble numerical weather predictions as input. Since the machine learning models use weather data as inputs and weather data have their own errors, providing a probabilistic forecast based on machine learning model uncertainty only would not be sufficient for capturing the actual variability of the predictions. A probabilistic framework based on weather ensemble forecasts would be the best candidate to capture the actual predictive uncertainty.

Finally, we would like to mention that, since the OPM is operational and emergency response personnel partially base their decisions on this outage prediction model, both the reduction of the model errors demonstrated in this paper, and future improvements have immediate social and economic benefits. Accurate outage predictions allow emergency managers to allocate the correct number of crews and equipment for preparing for upcoming storms. This results in shorter outage times, and reduces restoration costs. When the impact of a weather event is underestimated, higher restoration costs are associated with the need of calling out-of-state crews after the event. Moreover, crews travel time would delay the restoration process leading to longer outages. Higher costs are also associated with overestimation of a storm's impact, due to excessive crew allocation, therefore unnecessary restoration cost.

Chapter 3

Outage Prediction Models for Snow and Ice Storms

3.1 Introduction

Atmospheric icing is the accretion of precipitation, in-cloud droplets, or hoarfrost on the surface of an object [90], [91]. In recent years, several widespread power outage events have resulted from extreme atmospheric icing on electricity transmission and distribution networks caused by ice storms (including Wisconsin in 1976 [92]; Canada and the northeastern United States in 1998 [93], [94]; North Carolina in 2002 [95]; the Great Plains in 2007 [96]; and Hunan, China in 2008 [97], [98]) and wet snow storms (including Germany in 2005 [99], [100]; Spain in 2010 [101]; and the Northeastern United States in 2011 [102] and 2018).

The economic costs from such outage events have been enormous. In the United States, winter storm losses between 1988 and 1995 averaged $375 million (in 1997 U.S. dollars) per year, of which 60% were caused by ice storms [103], while losses from the 1998 ice storm in Canada were much higher. With 4.7 mil-

lion Canadians left without power, Hydro-Quebec and Ontario Hydro incurred repair costs estimated at Can$1 billion, while short-term losses in manufacturing, transportation, communication, and retail sales reached Can$1.6 billion, and income loss amounted to Can$1 billion [93]. In October 2011, a wet snowstorm in the northeastern United States left 3.5 million people without power [104], causing damages estimated between US$1 billion and $3 billion [105]. In Connecticut, costs for restoring power to 830,000 customers of CL&P (now Eversource Connecticut) amounted to US$175 million. More recently, in 2018, four powerful snowstorms again hit the Northeastern United States, each producing wet snow and ice that resulted in several hundreds of millions of dollars in damage and power outages lasting for several days.

Beyond economic losses, snow and ice storms causing widespread power outages produce health concerns. Outbreaks of carbon monoxide poisoning, produced mainly by the operation of charcoal grills and electric generators in the absence of power, occurred in Washington State between 1993 and 1996 [106], after the 1998 ice storm in Maine [107], after the 2002 ice storm in North Carolina [108], after the 2011 snow storm in Connecticut [109].

The prediction of atmospheric icing and its effects allows us to evaluate and adopt preventive measures and reduce calamitous losses like these [110]. To this end, several physical and empirical approaches have been used to model atmospheric icing (in the form of ice and snow accretion) on structures [111], [112].

Among them have been analytical, physically based models for estimating ice accretion: (i) a model based on heat transfer (wind and temperature) by neglecting precipitation intensity [113]; (ii) a model based on precipitation intensity only by neglecting all effects of wind and temperature [114]; a model based on wind speed and precipitation rate [115]; and (iv) models based on

wind and fall speed of the drops, and precipitation amount during the accretion time [116] and [117]. Also in use are numerical ice thickness models: a model based on wind speed, temperature, pressure, cloud liquid water content, droplet size distribution and wire size [118]; and a model based on temperature, wind speed, droplet diameter and liquid water content [119], an improved version of which is able to take into account cable diameter, angle between wind and line orientation, event duration, and formation of icicles [120].

Snow accretion on power lines was also widely investigated. According to [121], in dry conditions, snow accretion is limited to low- and medium voltage lines shielded against wind (less than 2 m s^{-1}), while in wet conditions heavy loads on power lines are associated with high precipitation intensities and above freezing temperatures. Wet snow accretion models ([122], [99], [123], [124]) have described accretion intensity as proportional to wind speed, sticking efficiency (proportional to wind speed [124]), snow terminal velocity, and concentration of wet snow in air (proportional to precipitation intensity [124], or to visibility [99]).

In the past two decades, researchers have begun to apply machine learning techniques to the prediction of ice accretion on overhead conductors. These have included the use of neural networks [125] trained on temperature, wind speed and direction, precipitation rate [126], [111] and humidity ([111] only). These studies concluded that the model 'gave unacceptable results' [126], and that 'precise point-by-point forecast seem[ed] unreasonable' [111]. More promising results were found with a Support Vector Machine (SVM, [127]) for learning ice accretion patterns using wind speed, wet bulb temperature, precipitation and fraction of frozen precipitation simulated in eight icing events by a Numerical Weather Prediction (NWP) model [112].

All these models predict icing accretion on power lines, but they do not pre-

dict the damage it will cause. A study that took a step further [28] employed a generalized linear mixed model (GLMM, [128]) to estimate the number of power outages in eight ice storms through the use of number of protective devices, ice thickness (from NWP simulations, using [115]'s ice accretion model) and ice storm indicator. Another advance in predictive modeling of snow impact was the use of more than fifteen explanatory variables to predict snow-related power outages through tree-based models [5], [6]. These ice and snow impact models belong to the broader category of storm outage prediction models (OPMs) developed as well for hurricanes [28], [5], [6], [18], [29], [31], [33], [34], [35], [37],[38], [19], [39], extratropical storms [5], [6], [1], and thunderstorms [5], [6], [1].

In outage prediction models, errors arise from both weather forecasting inaccuracies and limitations of statistical models [1]. With respect to snow and ice storms additional uncertainties arise from inaccurate prediction of precipitation type, primarily freezing rain and ice pellets [129], [130], [131], [132], [133], [134], [135], [136], [137]. An incorrect precipitation type prediction is magnified by an outage model for winter storms, since the impact of freezing rain in terms of power outages may be orders of magnitude higher than the impact of ice pellets, which do not accumulate on power lines.

In this study, we investigated the challenging task of snow and ice storm outage prediction through the use of statistical and machine learning techniques. In the following, a description of the study area and the methods for selecting and simulating the 54 snow and ice storms in our dataset is followed by an examination of the relationships among the snow- and ice- related variables for designing and validating two systems capable of predicting snow- and ice-related power outages. The two systems use variables quantifying the amount of leaves on trees, of freezing rain, snow and other precipitation types, of soil moisture, winds and gusts during storms, matching this information with soil type, eleva-

tion, land cover and infrastructure. Each system is cross-validated in different configurations using the entire dataset of snow and ice storms to find the optimal structure, based on the overall OPM performance evaluation. Prediction performance of the two systems are presented as errors between predicted and actual outages for each storm, and spatial maps of errors, in order to infer conclusions on the usefulness of each model for snow and ice storm preparedness by utility managers.

3.2 Datasets and study area

The outage prediction models developed through this work are based on variables related to weather, infrastructure, land cover, elevation and vegetation. The methods described for obtaining the variables composing our dataset are described in this section, while a detailed description of each input variable can be found in Appendix A.2.

3.2.1 Response variable

The response variable for the outage prection models is the number of outages occurring over a certain area. Electric utilities often keep records of power outages, and Eversource Energy-Connecticut (serving 1.2 million electric customers) provided us with an outage dataset containing geolocated power outages occurred between 2005 and 2018 in Connecticut. Each outage is defined as a location where a two-man crew is needed to restore power, and may affect several customers.

3.2.2 Storm list

The outage dataset represents the basis for the storm selection. Following the criteria described in [1], we identified snow and ice events as follows: (i) we identified the 95^{th} percentile of the daily outage distribution and we selected the storms producing at least 5 mm water equivalent of wintry precipitation over 25 percent of the territory; (ii) we added to this list the storms that produced a significant amount of wintry precipitation, but that were not associated with widespread outages. Through these principles, we selected 54 snow and ice events (listed in Appendix A.3) occurred in Connecticut between 2005 and 2018.

3.2.3 Predictor variables

Predictor variables describe weather and leaf conditions during storms; land cover, elevation and soil characteristics of the territory; and infrastructure.

Weather variables have been simulated, for each storm, using the Weather Research and Forecasting (WRF-ARW v.3.8.1 [47], [48]) NWP model. A WRF domain was set up for the Northeastern United States (Figure 3.1) at 4 km grid spacing. WRF simulations dynamically downscaled NCEP North American Mesoscale (NAM) 12 km analysis [138] over the domain of interest.

The WRF model configuration is described in Table 3.1. Each storm analysis started 12 hours before the beginning of the storm, lasting for 60 hours. A 12 hours spin-up time was then discarded, to obtain 48 hours of useful storm simulation. For each of the 803 Connecticut grid cells, weather conditions occurred during each storm were summarized into maximum, mean, and occurrence variables, reported in Appendix A.2. Among these variables, particular attention was given to the Air Force Weather Agency (AFWA) precipitation type variables, [139], such as snow, ice pellets, and freezing rain, since the focus of this study is to create a model for predicting outages in wintry conditions.

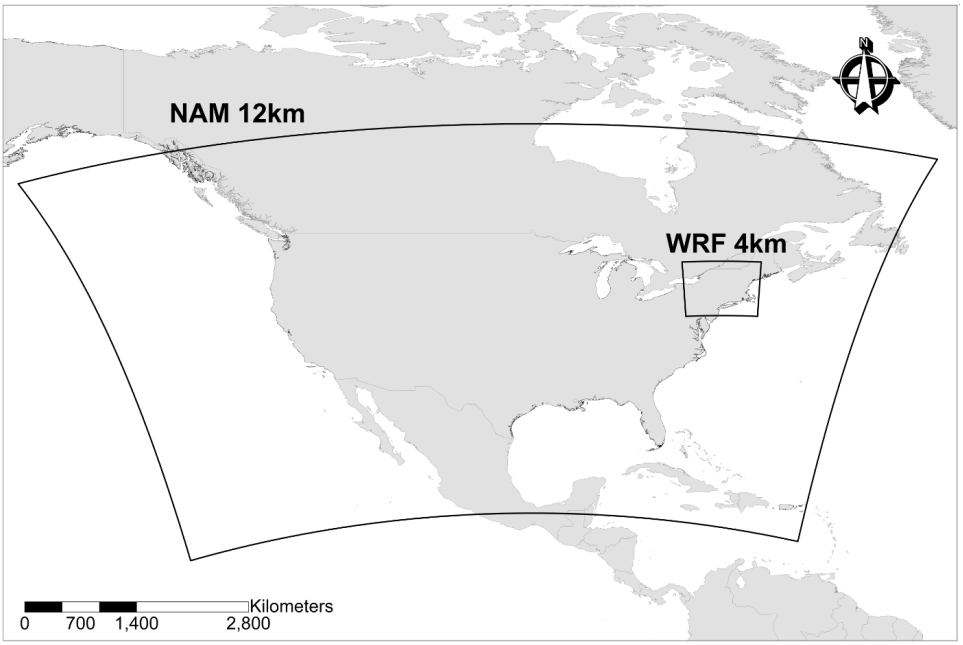

Figure 3.1: NAM 12 km domain, covering the entire CONUS, and WRF domain, centered on the Northeastern United States, with a 4 km grid spacing.

Parametrization	**Scheme**
Microphysics	New Thompson et al. [52]
Cumulus	Grell 3D Ensemble Scheme [53] [54]
Planetary Boundary Layer	Yonsei University [55]
Surface Layer	MM5 Similarity [56], [57], [58], [59] [60]
Land Surface Model	Unified Noah [61]
Longwave Radiation	RRTMG [140]
Shortwave Radiation	RRTMG [140]

Table 3.1: Parametrization schemes used in the WRF Model.

Infrastructure data are represented by the sum of isolating devices in each grid cell of the WRF model, since outages are usually reported to the closest isolating device. Land cover data (developed area, deciduous and coniferous forest) were derived from the National Land Cover Database (NLCD 2011, [141]). Similarly to [19], [39], [5], [6] and [1], data were aggregated into the WRF grid cells by considering only the land cover in proximity of overhead lines. Elevation was computed, for each cell, as the mean elevation of the overhead lines, from

the USGS 3DEP Digital Elevation Model (DEM) at 1 arc second resolution [142]. Soil data (hydric, sandy, rocky, depth of rocks) were derived from the USGS Soil Survey Geographic Database (SSURGO, [143]). Leaf Area Index (LAI) data were obtained from [1], who created a weekly climatological product by processing MODIS [67] observations.

3.2.4 Derived predictor variables

Beyond the variables mentioned above, we derived three new variables, from the WRF output, to model power outages associated with snow: *snow_density*, *snow_time* and *LAI_snow*.

Snow_density is a fundamental variable for discerning wet snow from dry snow events. Since the AFWA module provides both snow accumulation and snow water equivalent, it is possible to estimate snow density by computing the ratio between the snow water equivalent and snow accumulation.

Many icing accretion models are based on snow amount and wind speed. Since the weather variables extracted from WRF do not provide any information about the co-occurrence of wind and snow, a new variable, *snow_time*, was introduced as the ratio between the amount of snow fallen during the four hours of maximum wind, and the total amount of snow.

Lastly, since most of the power outages in Connecticut are caused by the interaction between vegetation and overhead lines, we introduced a quantity, *LAI_snow*, describing the combined effect of snow and vegetation amount, through the product of snow amount with LAI.

3.2.5 Snow and ice data analysis

In this section we analyze the winter storm dataset, with particular attention to understanding the role snow density may have on power outages. The 803

grid cells for each of the 54 winter storms analyzed in this study represent a large sample to infer important characteristics of the distribution of mixed-phase precipitation variables in Connecticut.

Histograms of snow (a), freezing rain (b) and ice pellet and graupel (c) for varying snow density (light, average and wet snow, delimited by red, vertical lines) are shown in figure 3.2. The value of 66.7 kg/dm^3 corresponding to a snow ratio of 15:1, is taken as reference point for the limit between light and average snow density [144], while the value of 105 kg/dm^3 (limit between average and wet snow) slightly differs from the 9:1 ratio (111.1 kg/dm^3) used in [144] due to technical reasons described in the next paragraphs. Dark bars in the histograms represent data associated with snow total amounts above 2.5 mm water equivalent (moderate snow, [145]).

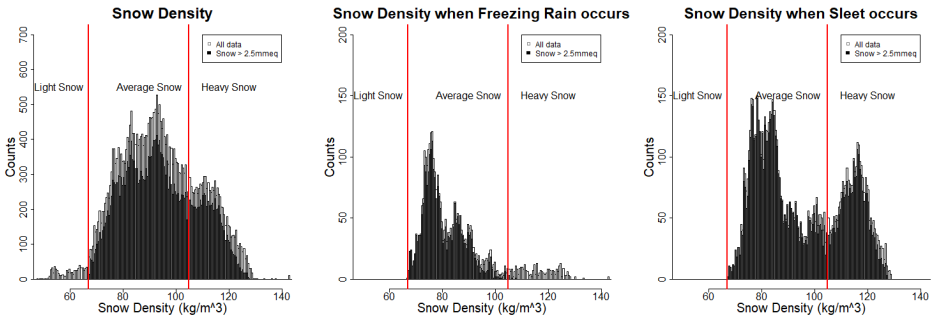

Figure 3.2: Histograms representing the number of records in the dataset with snow (left), freezing rain (center) and graupel or ice pellets (right) for varying snow density. Dark colors correspond to snow amounts above 2.5 mm w.eq., light colors to snow amounts below 2.5 mm w.eq..

From the histogram it is evident that most of the mixed-phase precipitation data for Connecticut correspond to average snow densities. Moderate amounts of dry snow never manifest (dry snow occurs for very low temperatures), freezing rain is never associated with moderate amounts of wet snow (freezing rain is associated with a low-level inversion, while wet snow with an isothermal profile), and sleet (comprising here both graupel and ice pellets) has a bimodal

distribution.

The reason why the limit between average and wet snow has been set to 105 kg/dm^3 is evident from Figure 3.3 a, b, c, where the mean number of outages per 100 assets is reported as a function of snow density. For snow densities below 105 kg/dm^3 we notice an inceasing, linear trend of mean outages for increasing snow density (Figure 3.3 a, b). Above this threshold, we note a sharp increase of outages in all storms, the most notable is for the 2011 nor'easter, which produced heavy snow on almost the entire service territory. In all cases, the peak of mean outages is around 115 kg/dm^3, and lower values can be found below 110 kg/dm^3 and above 120 kg/dm^3.

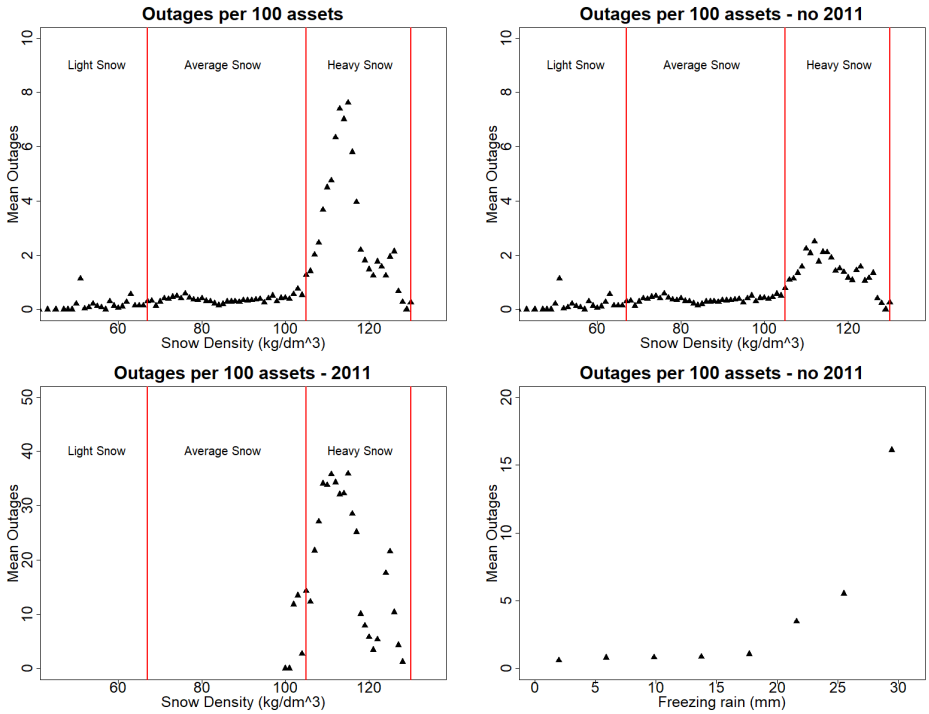

Figure 3.3: Mean number of outages per 100 assets by snow density for: (a) the entire dataset, (b) all the storms except for the 2011 nor'easter, (c) the 2011 nor'easter; (d) mean number of outages per 100 assets by freezing rain amount for all the storms except for the 2011 nor'easter.

There is therefore a well defined range of snow density values where storms can create large amounts of outages, and this range is between 110 kg/dm^3 and 120 kg/dm^3. This range is associated with temperatures between 1^{o}C and 2^{o}C (not shown). This result is consistent with [121], who found heavy snow loads associated with positive temperatures, due to capillary forces of liquid water and metamorphosis of snowflakes into ice, processes that are neglibile or absent at lower temperature. When temperatures are even higher, snow does not stick on power lines because either it is not able to freeze or it melts quickly. This behavior reflects in a sharp decrease of mean outages for snow densities above 120 kg/dm^3.

The effect of freezing rain on power lines is outlined in Figure 3.3d: no significant trend is evident for values below 20 mm (corresponding to 8 mm of radial ice accumulation, following [146]), while a strong outage increase is present for higher accumulation. The value of 8 mm of radial ice accumulation is not far from the value of 0.25 inches, used by the United States National Weather Service as threshold for an experimental product used between 2014 and 2015 for ice storm damage potential [147].

3.3 Methodology

This section describes the algorithms used for the outage prediction models developed for winter storms and the methods used for their validation.

3.3.1 Grid cell classification

In view of the uncertainties in precipitation type prediction and of the effects that different precipitation types have on power outages, we divided the storms dataset into three categories: (i) wet snow, (ii) freezing rain, ice pellets and graupel, and (iii) rain, wind and dry snow, based on the decision tree shown in

Figure 3.4.

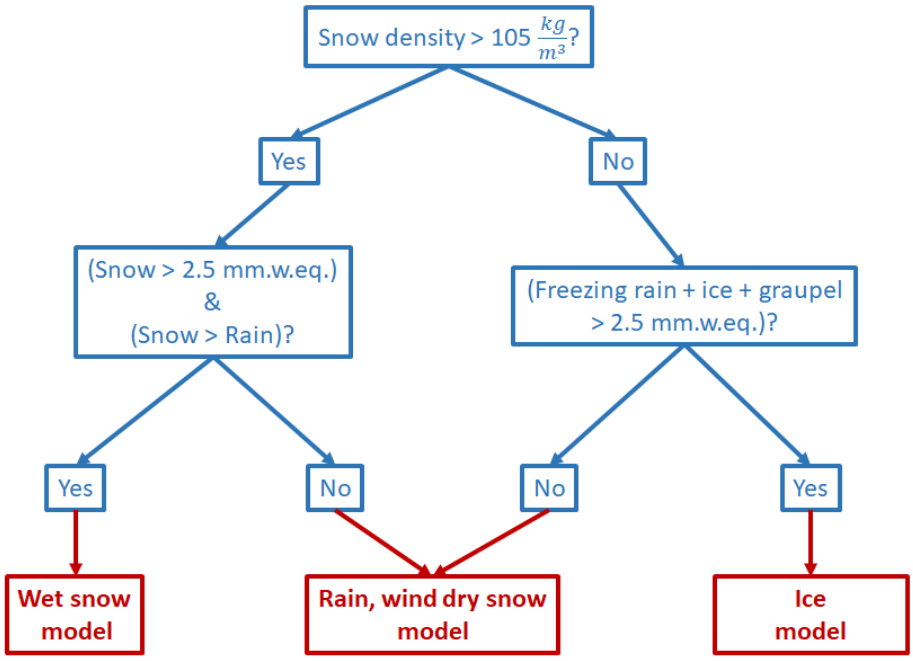

Figure 3.4: Algorithm for precipitation type classification.

The algorithm developed for precipitation type classification at a grid cell level follows the rules listed below:

- grid cells with snow density above 105 kg/dm^3 are isolated from the rest;
- for such grid cells, it is evaluated if a moderate amount of snow fell during the storm and if that amount was greater than the amount of precipitation fallen as rain. If these conditions subsist, these cells are classified as heavy, wet snow, otherwise as rain, wind and dry snow.
- for the grid cells that are not associated with high snow density, it is evaluated if a moderate amount of solid precipitation different than snow occurred. If this condition is valid, the cells are classified as ice, otherwise as rain, wind and dry snow.

Following this algorithm, all grid cells with moderate freezing rain (3.2b) are classified as ice; grid cells associated with the primary mode of the graupel and ice distribution (3.2c), co-occurring with average-density snowfall, are classified as ice too; and grid cells associated with the secondary mode are classified as wet snow, since almost all of them co-occur with moderate amounts of heavy snow (3.2c).

3.3.2 Machine learning models

We used the two best performing machine learning models utilized in [1], following the same configuration:

- a random forest (RF) model [32], formed by 200 decision trees. Each decision tree is able to split the dataset into subsets for which the response variable is similar, by minimizing the sum of the square error [72]. Each tree of the random forest is trained on a random subset of training data using a random subset of explanatory variables. The R package 'randomForest', based on [32], is used for this purpose;
- a Bayesian Additive Regression Tree (BART, [41]) model, obtained through statistical sum of thirty Bayesian trees, that are the base learners. A Markov Chain Monte Carlo (MCMC, [73]) algorithm is used with ten thousand iterations for fitting the BART model, and four thousand iterations are used for obtaining the predictions. The R package 'BART', based on [41], is used to run the model.

RF and BART were combined together through the optimization module described in [1] for obtaining a more robust model. The optimization consisted in the coefficient selection for the linear combination of the two models, by maximizing the ratio between the Nash-Sutcliffe Efficiency (NSE; [78]) and the median absolute percentage error (MdAPE).

3.3.3 Generalized linear model

In addition to the machine learning models, a simple Generalized Linear Model (GLM; [148], [149]) was tested for predicting power outages. GLMs represent an extension of linear models for non Normally distributed variables. In a GLM the response variable η_i is expressed as a linear function of multiple predictors plus an error ϵ_i:

$$\eta_i = \beta_0 + \beta_1 x_{1i} + \beta_2 x_{2i} + ... + \beta_n x_{ni} + \epsilon_i \tag{3.1}$$

where β_0 ... β_n are coefficients, a link function $g(\mu_i) = \eta_i$ describes the dependency of the mean $E(Y_i) = \mu_i$ on the linear predictor, and a variance function $var(Y_i) = \phi V(\mu_i)$ describes how the variance depends on the mean, with ϕ=const. Under the Poisson assumption, used for modeling the number of power outages at the town level, $Y_i = P(\lambda_i)$, then $E(Y_i) = \lambda_i$, $var(Y_i) = \lambda_i$ hence the variance function is $V(\mu_i) = \mu_i$, and the canonical link function is $g(\mu_i) = ln(\mu_i)$.

Despite a more complex model, the spatial generalized linear mixed model (GLMM), was used in [28], we opted for a GLM, because in [28] the authors concluded that models simpler than the spatial GLMM can produce similar estimates.

3.3.4 Cross-validations

ML and GLM outage prediction models were validated, similarly to [1], through leave-one-storm-out cross-validations. This method consists in predicting outages related to a storm using a model trained on all the other storms. In this study, multiple cross-validations were performed for obtaining the best configuration of each model: tests were performed with and without the grid cell classification module, at 4 km grid spacing and at a town level, and with dif-

ferent amounts of variables used as model predictors. The best performing configuration for each model is reported in Section 3.4, together with their performance.

3.3.5 Error metrics

The error metrics used for evaluating model performance were:

- the *median absolute percentage error* (MdAPE), for measuring the maximum percentage error committed 50 percent of the times;
- the *mean absolute percentage error* (MAPE), for measuring the average model accuracy;
- the *Nash-Sutcliffe Efficiency* (NSE; [78]), for determining the model efficiency for a number n of predictions P and observations O:

$$NSE = 1 - \left[\frac{\sum_{k=1}^{n}(P_k - O_k)^2}{\sum_{k=1}^{n}(O_k - \bar{O})^2} \right] \tag{3.2}$$

3.4 Results and Discussion

Several cross-validations have been performed in different configurations for the two predictive modelling systems. An overview of the GLM and ML configurations that produced the best results is presented in Table 3.2.

Feature	Configuration	**ML**	**GLM**
Predictive scale	4km	X	
	Town		X
Weather classification	Yes	X	
	No		X
Variables	Full list	X	
	Selected list		X

Table 3.2: Configuration of the ML-based and GLM-based models with the best performance.

Both the GLM and the ML systems were tested at the WRF model grid spacing of 4 km and at town level, by using or not the algorithm presented in Figure 3.4, and by decreasing the number of predictive variables with respect to the ones listed in Appendix A.2. The best performing ML-based system was the one at 4 km grid spacing, with weather classification at the grid level that used the full list of variables. On the other hand, the GLM model performance increased when data were aggregated at town level, without precipitation type classification, and with a more restricted list of variables. The last two elements can be explained as follows:

- the extension of the dataset drastically shrinks after aggregation to the town level, therefore a further classification would reduce the amount of data (especially for wet snow) to a level at which it would be difficult for GLM models to extract useful information. Moreover, over the territory of a town, precipitation type varies (e.g. between mountains and valleys) and the most common precipitation type is not representative for the entire town;

- a model is easily overfitted when the dataset size is small and the number of variables is large. This is the case for the GLM model with the full list of variables. After decreasing the number of variables, the model becomes well trained and there is a resulting performance boost in the cross-validation experiments.

In the following sections the variable importance for the best performing models is presented, together with models performance at service territory and at town levels.

3.4.1 Variable importance

Since variable importance is computed through different method across the different models, normalized importances are computed and presented in Figure 3.5. The variable importance plot for the machine learning models is provided for each of the three precipitation types, while for the GLM a single variable importance is presented, since the best performing model is not trained separately for different precipitation types.

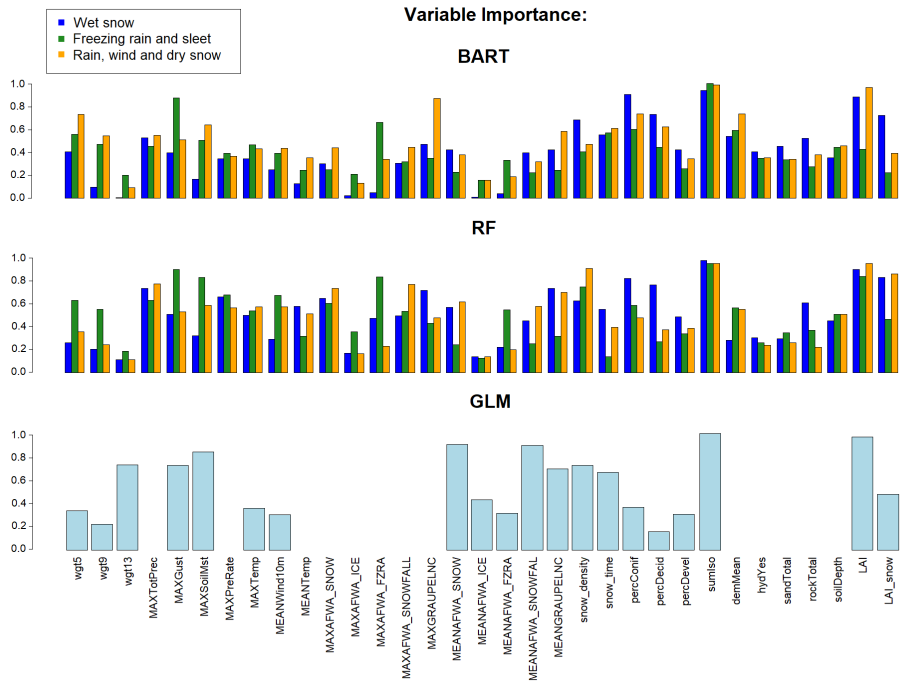

Figure 3.5: Variable importance for the BART, RF, and GLM.

All the models agreed on the two most important variables: assets on the territory and LAI. The first agrees with previous studies, since the number of failures is directly proportional to the number of assets that can fail. The second finding is connected to outage causality: trees are the primary cause of failures and the LAI allows the models to understand where wintry precipitation can

accumulate on trees, increasing the risk of power outages.

Beyond this agreement on the high importance of these two variables, other relevant findings can be summarized as follows:

- both machine learning models agreed in assigning a high importance to freezing rain and much lower to ice in the freezing rain and sleet model. Freezing rain in fact accumulates on trees and infrastructure, while sleet (ice pellets) does not. The importance of these variables is much lower in the GLM, since these variables are used for describing only on a small fraction of the dataset;

- the importance of coniferous and deciduous forest, and of the product between LAI and snow is high for the wet snow ML models, since those variables are related to vegetation caused outages;

- the high importance of snow density across all the models confirms its primary role, discussed in Section 3.2.5;

- maximum gusts are very important for all the models, since the interaction between gusts, trees and infrastructure, already discussed in [1], is a primary cause of outages. Gust is a parameter, beyond ice accumulation, used in the [147] ice accumulation index, and the high importance in the ice models developed in this work confirms its role.

3.4.2 Models performances

Differences in the principles of the ML- and GLM-based systems reflect in intrinsic performance differences that can be rationally explained.

Figure 3.6 provides a side-to-side comparison of the performances of the two outage prediction models in terms of storm total outages. In each scatterplot,

predicted versus actual outages are reported for each of the 54 storms, color coded according to the dominant precipitation type.

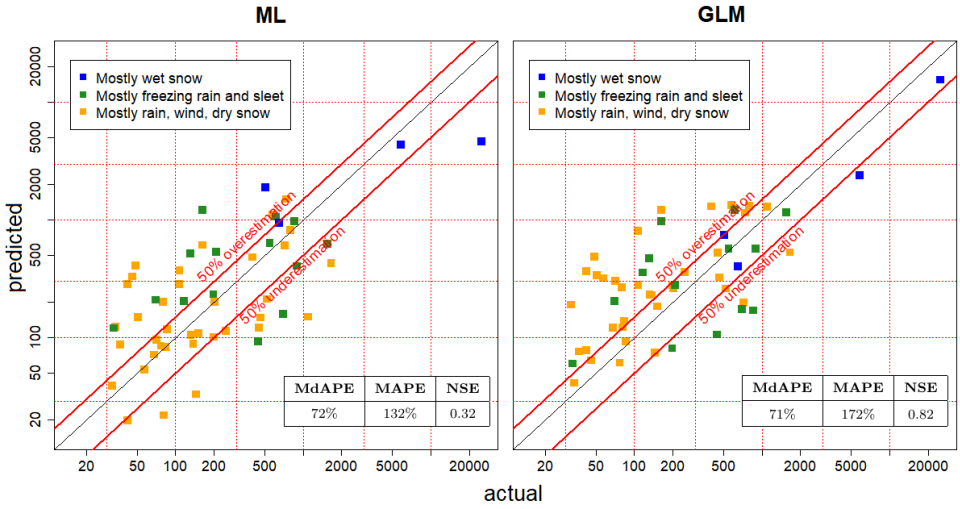

Figure 3.6: Cross-validation results for the ML-based and the GLM-based OPM.

Since both RF and BART models find patterns by classifying the data, it is not possible for the ML-based outage model to predict the most extreme event (the October 2011 nor'easter), because data of that magnitude are not present in the rest of the dataset. The GLM instead fits functions across variables, that can be potentially extended beyond the dynamic range of the training dataset. For the 2011 storm, the GLM-based model was able to extrapolate a value close to the actual, by using a training dataset in which the strongest event (March 2018) has a magnitude four times lower than the October nor'easter.

The GLM performances are generally better than ML models for medium- and high-impact events (above 300 outages), especially for wet snow events, while the GLM is biased for low-impact events, resulting in an overestimation of rain, wind and dry snow events. The OPM shower less variability for different precipitation types and magnitude for the ML-based model, since each precipitation type has its own unbiased model. The ML-based OPM has better

performance than the GLM for predicting the common low-impact events.

These visual characteristics are reflected in the performance statistics (shown on Figure 3.6): the high NSE of the GLM comes from the good prediction of strong events, while its higher MAPEis due to the very high relative errors in low-impact events prediction. The opposite is true for the ML-based models.

The spatial distribution of the error, provided in figure 3.7, highlights similarities but also differences between the two systems. For both OPMs, consistent overestimations are noted for the northwestern and southeastern Connecticut (areas where the number of assets, hence the expected number of outages, is lower), while underestimations can be found in the densely populated southwestern and central Connecticut. Error magnitude is generally higher for the GLM (darker colors), and lower for the ML (lighter colors), suggesting that the ML-based OPM is able to more accurately capture the spatial distribution of outages.

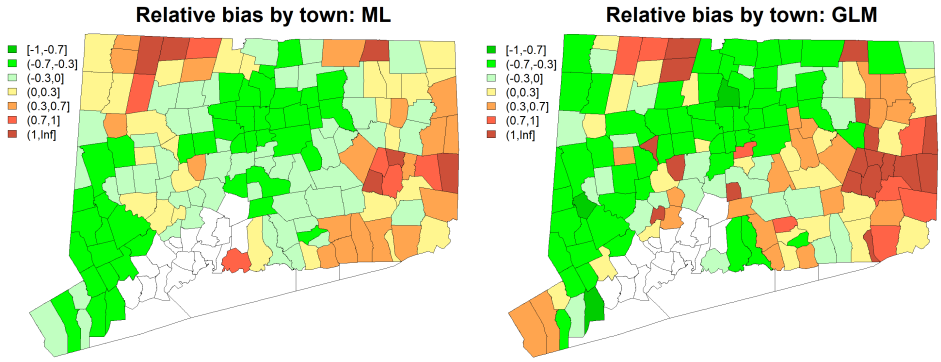

Figure 3.7: Relative bias for the ML-based and the GLM-based OPM.

The error characteristics of the two systems should be taken into account when model predictions are used for storm preparedness. Predictions with median errors around 70% may provide a relevant added value to the emergency preparedness personnel for taking preventive measures ahead of storm impacts.

It is well known, in fact, that utilities may be underprepared or totally unprepared (meaning underestimating the impact by one or two order of magnitudes) for the impact of strong events, since they do not have enough information for quantifying their impact (outages in our dataset span three orders of magnitude).

The two OPM systems proposed in this work would allow for a correct identification of very strong events and for a prediction of most of the medium and low-impact events within the magnitude of the actual outages. Model predictions should not be considered with full confidence, but as an indication of storm's impact severity, that may help allocating the right number of crews and resources for a prompt storm restoration.

It is also important to notice that this version of the models produces a spatial distribution of outages that is smoother than the actual distribution. A direct consequence of this characteristic is that model predictions should be enhanced, meaning that an even higher number of outages should be expected, on average, in locations where the model already predicts a high number of outages, while, on the other hand, a lower number of outages should also be expected in rural areas.

3.5 Conclusions

This study presented two systems for the prediction of power outages related to snow and ice storms, and evaluated their performance using 54 snow and ice events that occurred between 2005 and 2018. The machine learning based system used 33 variables, a precipitation type classifier, and an optimization module, to predict outages on a 4 km regular grid, using a random forest and a Bayesian additive regression tree model. The system based on a generalized linear model used 20 variables to predict outages at a town level.

From the analysis of the variable importance of the two systems it resulted that assets, leaf area index and snow density have the primary importance. These three variables describe the quintessential relationships between trees, weather and infrastructure. In the heavy snow model additional variables related to vegetation were important, while freezing rain amount and gusts were very important for the ice model.

The GLM model is able to correctly predict extreme events, while the ML models would underestimate the most severe nor'easter event. ML models have better performance than the GLM for the prediction of low impact events and have lower errors in terms of the spatial distribution of outages.

Both models are currently operationally used for predicting winter-related power outages for Eversource Connecticut. Future improvements of these models include the exploration of a possible blending of the two systems, for producing a new outage prediction model for snow and ice storms, capable of predicting extreme winter events, and valid also for capturing the spatial distribution of outages in low-impact events.

Chapter 4

Assessment of the Effects of a Vegetation Management Standard on the Rate of Outages in a Distribution Grid

4.1 Introduction

Electric utilities apply tree trimming and other vegetation management standards along power transmission [150] and distribution [151], [152] lines to minimize damages caused by trees during storms [25] and maintain system reliability [153]. Trees are among the top causes of outages in electric distribution systems

[154] [155], and vegetation management is a key component for improving the electric grid resilience to weather-related power outages [156].

In the absence of vegetation maintenance, trees can grow undisturbed and eventually fall on power lines [157], while cyclic tree trimming helps preventing trees and brush from interfering with the lines [158]. This cyclic vegetation management technique, which Eversource Energy-Connecticut performs every four to five years, is called Scheduled Maintenance Trimming (SMT), and consists in the removal of limbs within 8 feet (2.5 meters) to the side, 10 feet (3 meters) below, and 15 feet (4.5 meters) above the wires of the distribution lines [159]. Beyond SMT, Enhanced Tree Trimming (ETT) is also performed, and consists in the complete removal of trees and brush within 8 feet (2.5 meters) to the side of power lines [159].

Beyond the utility's perspective, tree trimming and removal in urban areas have climatological and societal dimensions: urban forests change microclimate conditions, by decreasing the temperature during hot summer days [160], [161], [162] and improving air quality [163] [164], [165], and also provide a more pleasant and comfortable living environment [166], [167]. Matching utility benefits with people' expectations in urban areas is challenging, because trees and overhead distribution lines share the same space [168]. Collaboration and coordination between utilities and municipalities is therefore needed to guarantee the reliability of the electric system consequently people' well-being [168], especially where public concerns about tree removal has been raised [169].Evaluation of the impact of ETT on power grid resilience may provide a vital piece of information for understanding the effects of this management practice.

A first attempt to evaluate the impact of tree trimming on failure rates for overhead (OH) distribution feeders can be found in [153]. According to that study, in a 8-year vegetation management cycle, there is a trend of increase of

failure rates between 3 and 7 years after tree trimming is performed. However, the high variability around the mean makes the results of this study quantitatively difficult to interpret. A reason for the lack of statistically significant results can be attributed to the absence of parameters describing the annual variability of storms impacts.

In nonstorm conditions, the effects of tree trimming on power outages were evaluated in [170], for an electric company in the Southeastern US. From the study it emerged, with statistical significance, that electric power system reliability is improved by tree trimming. Under storm conditions, a quantification of the reduction of the number of outages due to ETT has never been evaluated. However, it was demonstrated that tree trimming and other vegetation management techniques improve storm-related outage prediction [39].

This study aims at presenting methodologies for assessing of the ETT effects on the resilience of the electric grid. Specifically, we evaluate the impact of ETT on the rate of outages through two different approaches. The first is a purely statistical analysis of outage data to evaluate the trend of outage reduction to increasing ETT. The second is a resiliency evaluation carried out using an Outage Prediction Model (OPM) that predicts the power outages during storm events. The second approach allows to take into account the variability in storm severity through the use of OPM, which provides a reference for the evaluation. Results from the two evaluation frameworks will be compared against a straightforward assessment, which quantifies the change of outages for different tree trimming amounts without considering any other factor affecting power outage occurrence.

The next section provides a characterization of the dataset and a description of the model setup. Section 4.3 describes the methodology used for assessing the impact of ETT on electric grid resilience. The results obtained by following the

two methods proposed in this paper are presented and discussed in section 4.4. Finally, a summary of the principal findings of the study, together with their implications on future studies and the State economy is presented in section 4.5.

4.2 Model and Data

4.2.1 Variable description and Model Setup

This study is based on 100 extratropical storms exhibiting rain and wind conditions and 44 thunderstorms, occurred in the period 2005-2017 across Connecticut. The storms considered are an extension of the storm events dataset used in [5], [6] and [1] for OPM evaluation. The storm outage model was based on the combination of the two machine learning models that in [1] exhibited the best performance for outage prediction purposes: Random Forest (RF, [32]) and Bayesian Additive Regression Trees (BART, [41]).

Two hundred decisions trees [36] consitute our RF. Each decision tree is formed by a series of nodes and branches that split the dataset through decision rules, by minimizing the sum of square error. Each tree uses a random subset of predictor variables and is trained on a random subset of training data.

The BART model is a sum of tree models, that can be expressed as [41]:

$$Y = \sum_{j=1}^{m} g_j(x, T_j, M_j) + \epsilon. \tag{4.1}$$

where $m = 30$ is the number of binary trees T_j with associated sets of parameters M_j; x is the vector of predictors, ϵ is assumed to be normal, with standard deviation σ. The contribution $g_j(x; T_j, M_j)$ to the Bayesian sum provided by each tree is computed through ten thousand Bayesian iterations of the Markov Chain Monte Carlo (MCMC [73]) algorithm, starting from prior specifications for T_j, M_j and σ. Four thousand iterations are used after convergence is reached

to obtain the predictions. Number of iterations and trees are the same as [1], and are constrained by computational power.

The two models were trained on the storm datasets and used a number of input variables (described in Table 2.1) including weather, land cover, soil, vegetation, electric grid characteristics, and historical outages, similarly to [39], [5], [6], [19], and [1]. Weather and soil parameters were obtained from Weather Research and Forecasting (WRF v3.7) model [47], [48], operating in hindcast mode. The WRF model was initialized with Global Forecasting System (GFS) weather analyses and the dynamical downscaling occured through the use of three nested domains, at 18, 6 and 2 km grid spacing. Land cover variables weare obtained from the National Land Cover Database (NLCD) at 30 meters resolution, provided by the Multi-Resolution Land Characteristics Consortium (MRLC, [171]). Vegetation characteristics were represented through a Leaf Area Index (LAI) dataset, produced in [1]. This dataset was obtained through post-processing of a global LAI dataset [67] derived from MODIS [172] to compute, for every 8-day period of the year and for every grid cell, a climatological value of the LAI. Electric grid information, provided by Eversource Energy, included OH lines and annual tree trimming data. Storm outage data were provided by the electric utility: each outage is defined as a location where a two-man crew is needed to restore power, and the number of outages on a 2 km grid was the object of the models predictions.

4.2.2 Aggregation Methods

Our analysis was performed on the 2 km inner WRF grid. Weather- and soil-related variables, obtained from WRF output are already at the 2 km grid, but other datasets had to be interpolated to this grid. Land cover parameters, computed in the immediate proximity (60 m) of the OH lines, were aggregated for

each 2 km grid cell [19]. A similar procedure was employed for the computation of the OH trimmed and non-trimmed lines: the WRF grid was superimposed to the OH lines map, and the length of the lines in each grid cell was computed, together with the length of trimmed lines for each year (Figure 4.1). Consequently, for each cell and for each year, we computed the percentage of lines treated with ETT and the cumulative percentage of ETT from the beginning of the treatment.

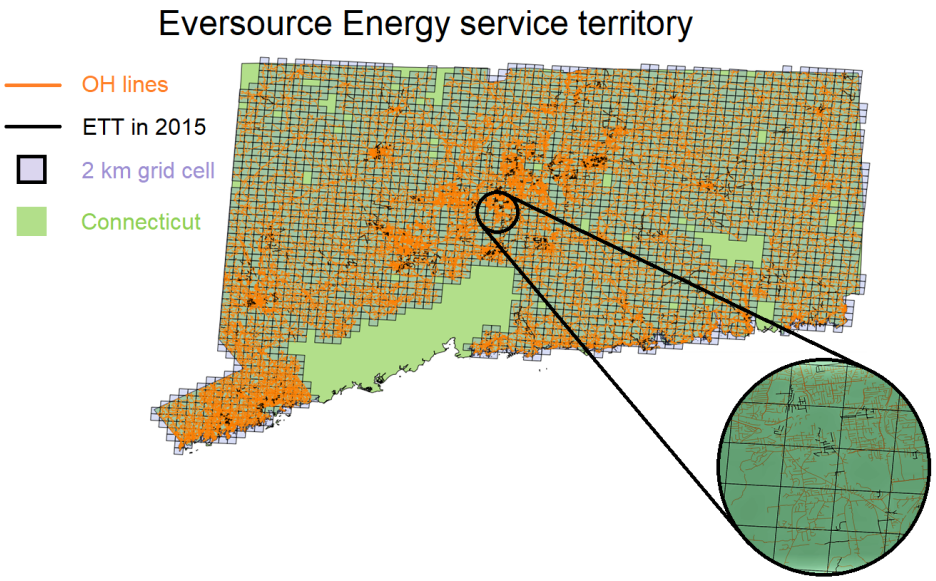

Figure 4.1: Map of overhead lines (orange) and ETTed lines (black) during 2015 in the State of Connecticut (green), with WRF model grid overlaid (squares).

To account for vegetation density characteristics we post-processed the LAI data by computing, for each grid cell and for each week of the year, the climatological value of the LAI through the use of a gaussian filter and an autoregressive model applied to the original, global dataset. All the outages measured during or in the immediate hours after each storm were attributed to the grid cell in which they were reported.

For analyzing the dataset at the town level, each grid cell is assigned to the

town with the largest areal coverage in the grid cell. Each town is assigned to a division on the basis of the geographic location (Eastern, Western, Southern, Central) within the utility service territory in Connecticut.

4.2.3 Dataset characteristics

The knowledge of the principal dataset features guided the development of the methods at the basis of the analysis performed in this work. In the following paragraphs we are presenting the characteristics of ETT and outage data, their mutual relationships, and the relationships with other variables of the dataset.

Between 2005 and 2008 ETT was not systematically performed, while between 2009 and 2016, ETT was performed on 21% of the total OH lines length in Connecticut, at a rate varying between 1.4% to 4.1% every year (Figure 4.2). The decision as to where to trim each year is affected by considerations, such as budgets and past reliability [3]. Between 2009 and 2017, 80% of the grid cells in the study area received some ETT in portions of the transmission or distribution lines they contain.

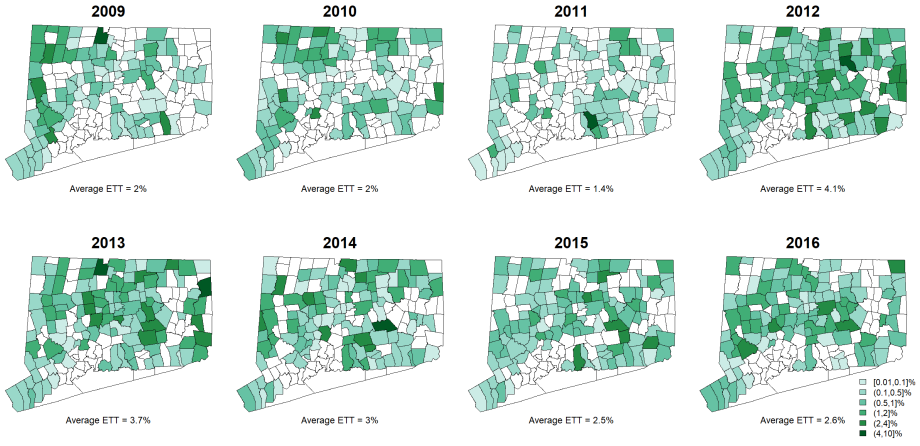

Figure 4.2: Percentage of ETTed lines by town in the State of Connecticut between 2009 and 2016.

Cumulative tree trimming amount presents a low variability across the 4 divisions, varying between 18% and 23%, and across the towns, since no town exceeds 50% of cumulative ETT (Figure 4.3a). Moreover, tree trimming is performed in both mostly forested and mostly developed areas (Figure 4.3a, 4.3b), hence no significant impact on the results of the analysis is expected from relating ETT to land cover variables.

The total number of outages for the considered extratropical storms and thunderstorm events is 58,236. Outages are primarily concentrated in South-Western Connecticut (Figure 4.3d), due to the high population and assets density. The outage temporal distribution is uneven across the years (Figure 4.3c) and the seasons. In particular, most of the dataset describes storms occurring when leaves are on trees, since the interaction between solid or mixed precipitation and the electric grid is not object of this study. Two major hurricanes (Irene, 2011; Sandy, 2012) have been excluded from the study, because their outage predictions require a different OPM, whose error characteristics are difficult to quantify due to the limited dataset. The strongest storm considered in our analysis, occurred on October 2017, produced 4430 outages.

The outage distribution is zero- and one-inflated: on average 91% of the grid cells in each storm do not contain any outage, 7% contain 1 outage, while less than 2% have a number of outages grater or equal than 2. For this reason, the study of the frequency of zeros versus non-zeros is an appropriate metric to describe the most important features of the dataset.

It is important to note that in each grid cell the total number of outages depends on the length of the OH lines (Figure 4.4a). The probability of having outages in a given cell is proportional to the line length in that cell. Moreover, also the cumulative ETT percentage depends on the line length, and the dependency of this quantity on the OH line length is shown for the year 2017 in

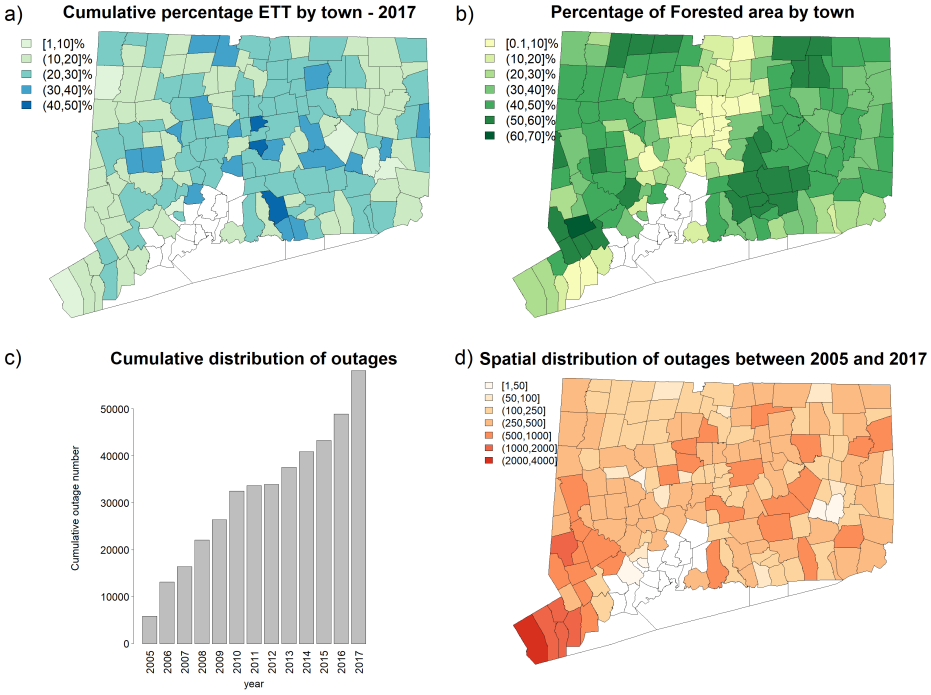

Figure 4.3: a) Cumulative ETT percentage as of 2017; b) percentage of forested area; c) cumulative and d) spatial distribution of outages between 2005 and 2017.

Figure 4.4b. All cells with total OH line length over 25 km are associated with cumulative ETT ranging between 5% and 55%, while all cells with ETT above 65% are associated with OH line length below 15 km. The first can be explained by the fact that if a grid cell has a high amount of OH lines it is more likely that a part of the lines was selected for the ETT program, but it is also less likely that all the vegetation next to the power lines was trimmed. On the contrary, it is more likely for a grid cell with a limited OH line amount to be completely trimmed.

Based on the above, one can argue that this relationship between ETT, outages, and line length can influence the results of this analysis. In the next section, we describe a methodology that, by taking into account these depen-

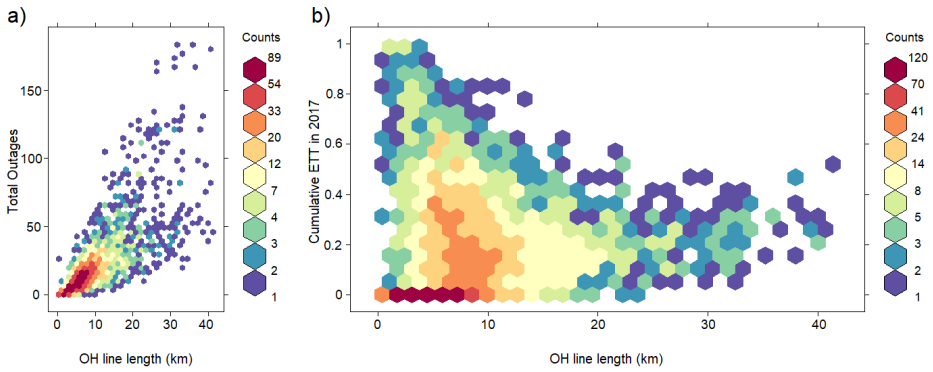

Figure 4.4: a) density scatter plot between total outage and OH line length; b) and between cumulative ETT fraction in 2017 and OH line length.

dencies, introduces corrections to the raw results. This approach is necessary for the correct interpretation of the ETT impact on the reduction of outages occurrence, and to avoid an overestimation of this impact.

4.3 Methodology

As discussed above, two separate methodologies were used to evaluate the role of ETT on the electric grid resilience:

- a statistical method, describing the relationship between the change of the number of outage-free grid cells and the amount of tree trimming.
- a model based analysis, which uses the OPM for establishing whether the impact of tree trimming on the amount of storm related power outages can be more accurately estimated by taking into account variations of storm frequency and intensity.

Both approaches were applied separately on the two storm types of this study: extratropical and summer thunderstorms. These methods are compared to a straightforward statistical assessment (hereafter named baseline), which

measures the percentage of outage free grid cells for different tree trimming amounts.

4.3.1 Baseline assessment

The first step for the analysis of ETT impact on power outages occurrence during storms was the selection of subsets of the original dataset with similar vegetation management characteristics. We set seven thresholds equally spaced between 0 and 100% of cumulative ETT per grid cell to create eight equal intervals. These intervals allowed us to partition the dataset, and to study the confidence intervals [LI, UI] for the proportions between the presence and absence of outages for each subset using the Wilson score interval with continuity correction [173] [174]:

$$LI = max\left\{0, \frac{2n\hat{p} + z^2 - \left[z\sqrt{z^2 - 1/n + 4n\hat{p}(1-\hat{p}) + (4\hat{p} - 2)} + 1\right]}{2(n + z^2)}\right\} \quad (4.2)$$

$$UI = min\left\{1, \frac{2n\hat{p} + z^2 + \left[z\sqrt{z^2 - 1/n + 4n\hat{p}(1-\hat{p}) - (4\hat{p} - 2)} + 1\right]}{2(n + z^2)}\right\} \quad (4.3)$$

where $z = 1.96$ for the 95% confidence level chosen, and $\hat{p} = n_z/n$ is the percentage of zeros, which is the ratio between the number of zeros n_z and the total number of entries n.

This baseline evaluation of the ETT change among the subsets, produces both deceiving and inaccurate results, by misrepresenting the impact of ETT, due to the lack of normalization for OH line length and storm intensity. We will use the baseline results as a starting point of our analysis, and we will compare the results of the herein proposed methods with the findings of this baseline

evaluation.

4.3.2 Statistical data analysis method

In order to provide a more accurate evaluation of the ETT impact on electric grid resilience, we investigated some important factors affecting the occurrence of power outages through a statistical approach.

The change of the percentage of zeros between the subsets is only partially explained by a different tree trimming amount. The principal reason for the change of this percentage is given by the dependency between ETT and OH lines, already introduced in Figure 4.4. The boxplots summarizing the principal characteristics of the OH line length distribution computed for all the storms across the subsets (Figure 4.5) show a strong decrease of OH line length per grid cell for increasing ETT, if tree trimming is performed. Since the expected number of outages is proportional to the OH line length, the strong decrease of OH line length for increasing ETT suggests, per se, a modification in the expected number of outages. For this reason, it was necessary to perform the following steps:

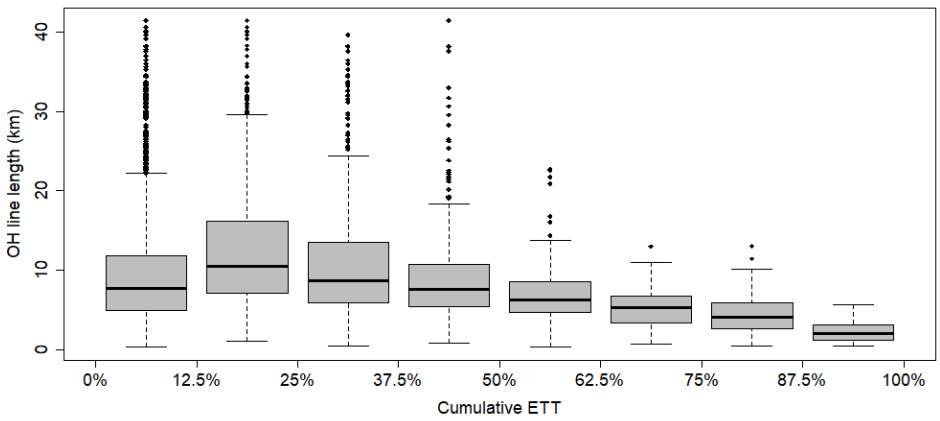

Figure 4.5: Boxplots of OH line length for each subset based on ETT amount.

1. To control our experiment we created new subsets for each tree-trimming interval using the outage history of the grid cells. For each member of the partition studied in the baseline assessment, the new subsets contain the history of weather, outages and trimming for the grid cells of this member. Since all the grid cells had a starting value, before 2009, of 0% ETT, the first subset, corresponding to [0%,12.5%] ETT, contained the entire dataset, and was not considered in this part of the analysis. For each other subset, the ETT histogram was composed of two peaks, that can be identified as before and after ETT. For each peak, we computed the confidence interval on $\hat{p}$ using the Wilson score. Multiple sessions of ETT were identifiable as background signal in the histogram.

2. We computed the quantity F of outage-free grid cells per standard OH line length:

$$F = \frac{\hat{p} * m}{l} \tag{4.4}$$

   where $m = 9.4km$ is the mean OH line length for all the grid cells, and l is the mean length for the considered subset. This normalization allowed us to take into account of the relationships between the number of outages and the length of the OH lines.

3. We computed the coefficients a and b, and their respective standard errors, both before and after ETT was performed. For this purpose, we used a weighted linear least square regression model [175] for the dependency of F on the ETT intervals:

$$F = a + b \cdot ETT + \epsilon \tag{4.5}$$

where a is the intercept, b is the slope and ϵ the vector of errors. Values different than zero for the slope correspond to the presence of a trend in the number of outage-free grid cells for varying tree trimming. The intercept a can be associated to a typical value for the number of outage-free grid cells, therefore changes in a correspond to changes in reliability between before and after tree trimming.

4. We performed a z test for the slope of the regression, following [176] and [177]:

$$Z = \frac{b_1 - b_2}{\sqrt{SE_{b_1}^2 + SE_{b_2}^2}} \tag{4.6}$$

where b_1 and b_2 are the slopes of the regression models respectively before and after ETT, and SE_{b_1}, SE_{b_2} their standard errors. The test for the slope allowed us to draw conclusions about the presence of possible trends of outage reduction for increasing tree trimming.

The statistical approach described above is used to evaluate the impact of ETT on the number of outage-free locations. However, since the number of power outages depends on storm intensity, the statistical analysis of the outage dataset alone is not sufficient due to the variability of number and severity of storms each year and the impact this variability has on the results. Therefore, this analysis was extended using the OPM model, that allows to normalize the outages based on the expected number for each storm. This method is discussed in the next section.

4.3.3 OPM Model Based Method

The trends and the associated uncertainties in the number of outages, and their dependencies on storm intensity, OH line length, and ETT can be simultane-

ously considered by using the OPM. Specifically, the OPM ability to predict the intensity of storm impacts based on weather, land cover, soil moisture, vegetation variables, and electric grid characteristics allows to take into account of the storm severity variability by studying the relationships between predicted and actual outages.

The evaluation process of ETT impact on outage reduction through the use of the OPM consists of the following stages:

1. For each subset of the partition introduced in subsection 4.3.2, we computed the mean number of OPM predicted and actual outages per grid cell per storm. Following [178], the 95% confidence intervals for the mean were calculated as:

$$CI = \bar{x} \pm t_{\alpha/2}(s/\sqrt{n}) \tag{4.7}$$

   where $\bar{x}$ is the mean, $t_{\alpha/2}$ is the critical value of the t-distribution, s is the standard deviation of the data, and n the number of samples.

   From the analysis of the trends of actual and predicted outages, it was possible to understand the model behavior for the different storm types.

2. Following the procedure performed in subsection 4.3.2, we analyzed the family of subsets for an evaluation of the change of outages in locations where ETT was performed. For each subset, the Outage Overestimation Factor (OOF), was computed as the ratio between the predicted and the actual outages per grid cell. This quantity is invariant for both storm intensity and OH line length, and is close to 1 (unbiased) when computed on any sufficiently large dataset. However, ETT is not a variable used in the OPM, hence the OOF provides information on the outage reduction where ETT was performed.

Since the number of outages is much smaller than the number of entries in the dataset, and since in only 2% of the locations the number of outages is greater than one, a good approximation for the confidence intervals for the OOF is given by the confidence interval for the risk ratio. The lower and upper boundaries can be computed, following [179], as:

$$[LI, UI] = OOF \cdot exp\left(\pm z\sqrt{\frac{1}{x_1} - \frac{1}{n_1} - \frac{1}{x_2} - \frac{1}{n_2}}\right) \tag{4.8}$$

where x_1 and x_2 are the numbers of predicted and actual outages in each subset, that can be approximated as the number of grid cells with outages, and $n_1 = n_2$ is the dimension of each subset.

Since the results obtained for the absence of ETT are statistically unbiased, there is no need to proceed to further post-processing.

4.4 Results

Using the above-mentioned methodology, in this section we will quantify the impact of ETT on storm related outage frequency. We will compare results from the statistical and modeling approaches, for both thunderstorms and extratropical storms, in order to explain similarities and differences between storm types and approaches.

The first step of our analysis consisted in the assessment of the change of the number of outages per grid cell per storm and of the percentage of zeros for increasing ETT. For this purpose, we selected the subsets of the partition introduced in section 4.3.2, and we computed means and confidence intervals of the quantities of interest. For both extratropical storms (Figure 4.6, left) and thunderstorms (Figure 4.6, right), we determined, with statistical significance, a decrease of the number of actual outages per grid cell per storm (Figure 4.6,

top), and an increase of the percentage of outage-free grid cells in the dataset (Figure 4.6, bottom) for increasing ETT. These results allowed us to estimate a 10 fold (87% to 91%) decrease of the number of power outages between the first and the last subset. It is important to note here that the OPM was able to predict the decrease of the number of outages for increasing ETT (Figure 4.6, blue markers), although this quantity was not used as model predictor. This finding suggests that the predictability of the decrease of outage frequency for increasing ETT can be mostly explained by the decrease of OH line length for increasing ETT (Figure 4.5), and by the relationships between outages and OH line length (Figure 4.4a,b).

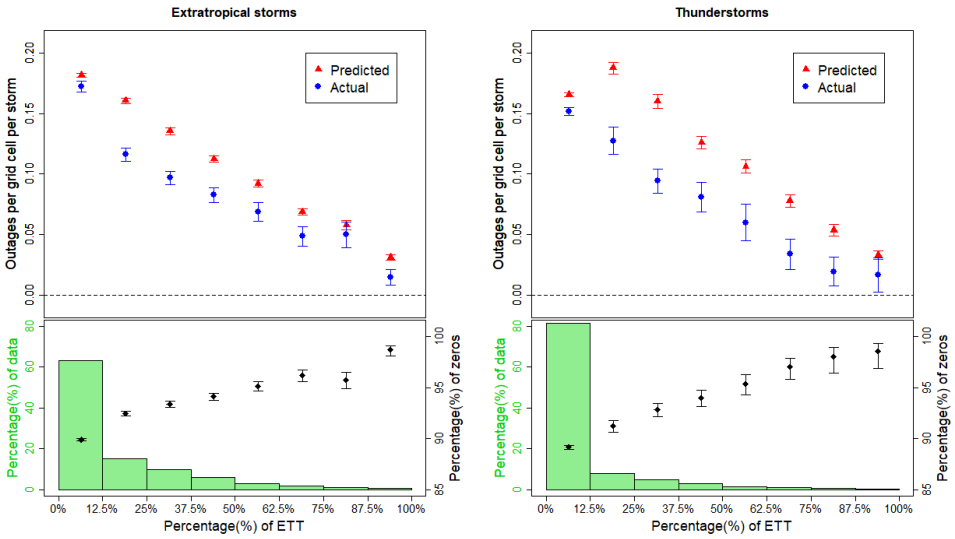

Figure 4.6: Trend of predicted (red) and actual (blue) trouble spots versus the percentage of tree trimming (top); percentage of data (green) and percentage of zeros (black) for varying tree trimming (bottom), for extratropical storms (left), and thunderstorms (right).

The OPM predictions, however, present an ETT-dependent bias, which manifests as an increasing overestimation of the average predicted outages with respect to the average actual values. In order to extract information from the bias

change, we investigated the change of the OOF, already introduced in section 4.3.3, between before and after ETT being performed. It is noted that, for all the considered subsets, the value of the OOF was not significantly different than the target value of one (unbiased) for the data corresponding to storms hitting areas of the territory before ETT was performed. For the same locations, however, the OOF was significantly different than one after trees were trimmed, for all the subsets, except for (75%,87.5%] ETT, as shown by the blue markers in Figure 4.7. These results allowed us to estimate that the impact of ETT on outage occurrence could be quantified as a 16% to 48% reduction in outage frequency (36%-63% for thunderstorms, 13%-52% for extratropical storms, not shown). We did not find, however, any statistically significant trend (not shown) of increase of OOF for increasing ETT, despite the group with the highest ETT amount presenting the highest OOF value.

For the same subsets, we also studied the change of actual outage-free grid cells before and after tree trimming. By contrasting the percentage of zeros within each subplot of Figure 4.7, we found a significant increase of outage-free grid cells for all the groups after ETT was performed. Moreover, from a comparison across the different subplots of Figure 4.7, we noticed that a strong increase was also present across different groups.

Through the information brought about by the differences across the groups, we quantified the average ETT impact, and the dependency of this impact on the amount of ETT. To achieve this, we computed the quantity F (equation 3), which allowed us to normalize the percentage of zeros across the ETT groups, and to evaluate whether the differences within the groups varied across the groups. It is important to note that the larger widths of the confidence intervals associated with high ETT values is due to the smaller sample size of these classes (green histograms in Figure 4.6).

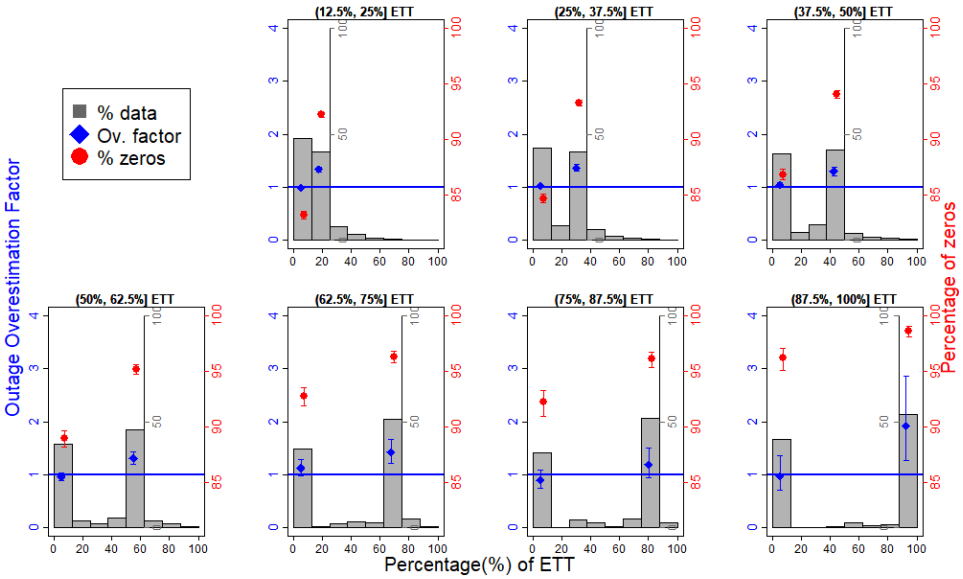

Figure 4.7: Change of power outage frequency between before and after ETT is performed, for varying ETT amounts. The blue squares represent the change in the OOF, the red circles represent the change of the number of outage free grid cells. Both quantities are computed before (left peak of each histogram), and after (right peak) ETT is performed. The background noise of the histogram corresponds to multiple ETT in the same grid cell during the years.

From this analysis we found that:

- for both extratropical storms and thunderstorms, a significant increase of the number of outage-free grid cells was measured after ETT was performed. This increase, according to Figure 4.8, corresponded to an average decrease of grid cells with outages, ranging between 43% and 69% for thunderstorms , 50% and 67% for extratropical storms, and 49% and 65% for the combination of the two.

- the areas that received tree trimming were associated with a lower normalized percentage of zeros before ETT. This means that ETT was correctly performed in the most vulnerable areas;

- for both extratropical storms and thunderstorms, the slopes of the weighted

linear regression models before and after ETT differred each other at $\alpha = 0.05$ confidence level. The Z value for the difference in slopes for the dataset obtained by the combination of extratropical storms and thunderstorm was Z=-2.25. This finding implied that, under the assumptions valid for this statistical analysis, the higher the cumulative ETT is, the higher its impact on outage reduction will be.

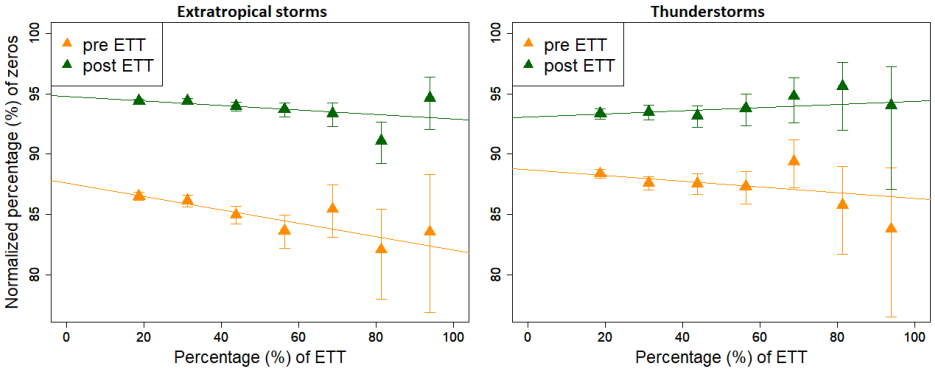

Figure 4.8: Normalized percentage of zeros for varying ETT before (orange markers) and after (green markers) ETT was performed, for extratropical storms (left) and thunderstorms (right), with weighted linear least square regression lines overlaid.

This last result based on the count of outage-free grid cells contradicts the absence of trend of OOF for increasing ETT. The difference between these two findings could be explained by the different assumptions used and by the different quantities involved, and more in detail:

- despite the vast majority of the grid cells had zero or one outage per storm, 2% of the cells had more than one outage. A reduction of outages due to tree trimming in highly impacted grid cells did not affect the statistics for presence/absence of outages, but did affect the OOF;
- we assumed that the use of the OPM produced a normalization for storm intensity, and was able to remove temporal inconsistencies in the dataset,

due to a varying storm selection across the years, or a trend of storm intensity. This assumption was not valid for the statistical method;

- the Z value (equation 5) of -2.25 was very close to the threshold of rejection of -1.96. This means that the conclusions on statistical significance could be reversed by assuming a 3-sigma limit instead of a 2-sigma.

Moreover, the lack of a clear trend in the increase of reliability for increasing tree trimming may be explained by the fact that not all power lines are placed next to trimmable trees. Consequently, similar increases are found (not shown in this paper) for locations where different amounts of ETT were performed, but corresponding to the same percentage of trimmed overhead lines.

Similarities in the results between the two approaches consist in the statistical significance of the average impact of tree trimming on power outage. By combining the results from the two methods we estimate, under different assumptions, that ETT produced a 16% to 65% reduction of the number of power outages.

4.5 Conclusions

The comparison performed in this work between the statistical analysis of the number of outage-free grid cells and of the OOF provided an improved understanding of the relationships between ETT (a vegetation management standard in Connecticut that represents removal of trees within 8 feet of power lines), outages, line length and storm severity.

The analysis of the data started with a direct evaluation of the reduction of the number of outages and of the increase of outage-free grid cells due to tree trimming. Using such a simplistic approach, we estimated a 10 fold decrease of the number of outges in extensively trimmed areas, with a significant trend of

outage reduction for increasing ETT.

However, highly trimmed areas corresponded to areas with a lower OH line length, where a lower value of power outages was expected. By taking into account the OH line length in the study, we found that most of the outage reduction variability was explained by this quantity, and tree trimming accounted for a 49% to 65% reduction of grid cells with outages, with a statistically significant outage reduction trend for increasing ETT.

This approach did not take into account the variability of storm intensity. For this reason, we used an OPM to estimate the change in the OOF for different ETT ranges. The ETT impact on outage reduction based on this method was estimated between 16% and 48%. However, the model overestimation did not show any statistically significant trend for varying ETT (results are summarized in Table 4.1).

Method:	**ETT only:**	**Statistical:**	**Modeling:**
Outage reduction: Thunderstorms	87% - 89%	43% - 69%	36% - 63%
Outage reduction: Extratropical	87% - 91%	50% - 67%	13% - 52%
Outage reduction: Combined	87% - 91%	49% - 65%	16% - 48%
ETT amount (slope): Thunderstorms	signif.	signif.	not signif.
ETT amount (slope): Extratropical	signif.	signif.	not signif.
ETT amount (slope): Combined	signif.	signif.	not signif.

Table 4.1: Summary of the principal findings of this work.

Further investigation is needed to explore the high variability in the relationship of ETT and outage rates. In a future study we will use a LIDAR-derived product describing the proximity of trees to power lines [39] as proxy to trimmed and trimmable areas, and use this dataset to study the change of reliability for varying trimmed areas.

The framework presented in this work will inform utilities as well as regulators and town officials about the efficiency of vegetation management programs in terms of improving the reliability of the system, and consequential financial

benefits from reduction of outage rates. The continuation of this study will focus on outage reductions to economic benefits continuation of this work, and a step forward for the definition of optimal vegetation management and urban planning strategies for maximizing the benefits for utilities and its ratepayers.

Moreover, the OPM can benefit from an extension of this study through:

- the implementation of the expected reduction of outages due to ETT, which may provide corrections to the model in areas of significant trimming;
- the use of ETT as a predictor, in order to quantify outage variability due to tree trimming.

Chapter 5

Concluding Remarks

This disseration contributes to the understanding of the interactions between environmental factors and the overhead distribution network through the creation and improvements of outage prediction models (OPMs). This works also opens the way to the use of new methodologies involving OPMs for the evaluation of resiliency improvements performed on the electric grid.

The first achievement of this study was the implementation of new modules in existing outage prediction models for the simulation of extratropical storms and thunderstorms. The introduction of three modules - storm classification, model optimization, and leaf area index - led to OPM versions significantly improving the predictive skill of the model. Most of the extratropical storms were predicted within 47% error, and most of the convective storms within 29% error. The reason of the lower error for the convective storms is the smaller range of outages associated to these events (they are, on the contrary, more difficult to predict, as suggested by their lower Nash-Sutcliffe efficiency). Performances of the OPM models were also tested in forecasting and analysis mode. Similar performances found through an error analysis in both configurations led to the

conclusion that a system trained on analyses and using weather forecasts is technically and operationally valid.

The second accomplishment of this work consisted in the creation of two OPMs for predicting power outages during snow and ice storms. The first OPM, based on machine learning models, was used to predict power outages on a 4 km grid; the second OPM, based on a generalized linear model, was used to predict outages at a town level. Assets, leaf area index, and snow density were consistently the most important variables in all models. During heavy snow conditions, additional variables related to interaction of vegetation and snow were important for the machine learning based model, while freezing rain amount and gust were important when ice was expected to accumulate on power lines. Extreme events were better predicted by the generalized linear model, while low impact events were better predicted by the machine learning model, characterized also by better error metrics.

Finally, an assessment of the role of enhanced tree trimming (ETT) for power grid resilience during extratropical storms and thunderstorms was conducted. The assessment involved two approaches: a pure statistical analysis of the number of outage-free grid cells before and after ETT was performed, and an analysis of the change of the number of outages before and after ETT, by taking into account the variability of storm intensity, through the OPM. According to the first approach, ETT was responsible for a 49% to 65% reduction of grid cells with outages. By taking into account the variability of storm intensity through the OPM, the role of ETT decreased, resulting in a 16% to 48% reduction of the number of outages across the Connecticut service territory.

The OPMs for thunderstorms, extratropical storms, and snow and ice storms developed in this work have a vital role for storm preparedness and response. OPM predictions allow managers to be informed about impacts of storms asso-

ciated to various weather conditions. This information helps managers to decide on the preventive measures needed to prepare for the impact and to reduce the costs associated to restoration. The estimation of the role of vegetation management on electric grid resilience helped to quantify the benefits deriving from tree trimming in terms of power outage reduction. This study is the first step towards a cost/benefit study and for planning optimal strategies for improving electric grid resilience.

Appendix A

Appendix

A.1 Error metrics

The error metrics are listed below:

- The *median absolute percentage error* (MdAPE): maximum percentage error that can be committed 50 percent of the times.
- The *mean absolute percentage error* (MAPE):

$$MAPE = \frac{1}{n} \sum_{k=1}^{n} \left| \frac{F_k - O_k}{O_k} \right| \tag{A.1}$$

- The *Pearson product-moment correlation coefficient* (r): linear correlation between predictions and observations.
- The *normalized standard deviation* (NSD): ratio between the standard deviation of the model and the standard deviation of the observations.
- The *normalized centered root mean squared error* (NCRMSE) measures

the random component of the error:

$$NCRMSE = \sqrt{\frac{\sum_{k=1}^{n}\left[(F_k - \bar{F}) - (O_k - \bar{O})\right]^2}{\sum_{k=1}^{n}\left[(O_k - \bar{O})\right]^2}} \tag{A.2}$$

- the *Nash-Sutcliffe Efficiency* (NSE; [78]), a nondimensional measure of efficiency, ranging between $-\infty$ and 1, that determines the magnitude of the residual variance of a regression analysis relative to the initial, observed variance:

$$NSE = 1 - \left[\frac{\sum_{k=1}^{n}(F_k - O_k)^2}{\sum_{k=1}^{n}(O_k - \bar{O})^2}\right] \tag{A.3}$$

where, for all the metrics, n is the total number of storms, F_k and O_k are respectively the k^{th} prediction and observation, and $\bar{O}$ the mean observed data.

A.2 Variable description

Variable [Units]	**Description**
Wgt5, 9, 13 [hr]	Duration of wind at 10 m above 5, 9, 13 m/s
MaxTotPrec [mm]	Total precipitation
MaxGust [m/s]	Maximum wind gusts at 10 m
MaxSoilMst [mm mm^{-1}]	Maximum soil moisture
MaxPreRate [mm h^{-1}]	Maximum precipitation rate
MaxTemp [K]	Maximum temperature
MeanWind10m [m s^{-1}]	Mean wind at 10 m
MeanTemp [K]	Mean temperature during 4 hrs of max wind
MaxGraupelnc [mm]	Total graupel accumulation
MeanGraupelnc [mm]	Graupel accumulation during 4 hrs of max wind
MaxAFWA_snow [mm]	Total liquid equivalent snow
MaxAFWA_ice [mm]	Total ice pellet accumulation
MaxAFWA_fzra [mm]	Total freezing rain accumulation
MaxAFWA_snowfall [mm]	Total snow accumulation
MeanAFWA_snow [mm]	Liquid equivalent snow during 4 hrs of max wind
MeanAFWA_ice [mm]	Ice pellet accumulation during 4 hrs of max wind
MeanAFWA_fzra [mm]	Freezing rain accumulation during 4 hrs of max wind
MeanAFWA_snowfall [mm]	Snow accumulation during 4 hrs of max wind
Snow_density [kg m^{-3}]	Snow density
Snow_time [-]	ratio between snow during 4 hrs of max wind and total snow
LAI_snow [%]	Product between LAI and total snow
PercDecid [%]	Percentage of deciduous forest
PercConif [%]	Percentage of coniferous forest
PercDevel [%]	Percentage of developed area
DemMean [m]	Mean elevation
HydrYes [%]	Percentage of hydric soil
SandTotal [%]	Percent of sand in soil
RockTotal [%]	Percent of rock in soil
Soil depth [m]	Mean soil depth
SumIso [-]	Total number of isolating devices
LAI [m^2 m^{-2}]	Leaf area index

Table A.1: Description of the predictor variables used in the data set.

A.3 Storm lists

Extratropical storms							
Date	**Outages**	**Date**	**Outages**	**Date**	**Outages**	**Date**	**Outages**
2005-09-29	557	2010-04-28	575	2014-11-02	648	2016-01-28	24
2005-10-15	712	2010-05-07	815	2015-01-07	63	2016-02-13	127
2005-10-24	754	2010-09-29	1366	2015-08-06	45	2016-02-15	534
2006-01-17	2918	2011-12-07	709	2015-08-11	184	2016-02-19	92
2006-02-16	302	2013-01-30	1921	2015-09-10	223	2016-02-28	63
2006-06-06	531	2013-05-11	37	2015-10-25	89	2016-03-01	114
2006-09-01	1299	2013-05-23	310	2015-10-28	490	2016-03-17	71
2006-10-27	891	2013-05-25	235	2015-11-06	84	2016-03-28	228
2006-11-30	330	2013-06-07	158	2015-11-12	243	2016-04-07	82
2007-04-14	1141	2013-06-13	157	2015-11-18	191	2016-09-04	295
2008-03-08	659	2013-10-31	219	2015-12-03	55	2016-09-23	94
2008-03-20	220	2013-11-18	77	2015-12-14	110	2016-09-28	68
2008-10-25	1419	2013-11-26	355	2015-12-19	53	2016-10-24	65
2008-12-24	135	2014-01-06	81	2015-12-23	104	2016-11-03	64
2008-12-30	408	2014-04-14	346	2015-12-28	55	2016-11-11	132
2009-05-09	112	2014-05-16	153	2016-01-03	97	2016-12-08	68
2009-10-06	1065	2014-06-18	184	2016-01-09	217	2016-12-12	72
2009-11-27	396	2014-10-08	137	2016-01-15	99	2016-12-14	121
2010-03-13	3590	2014-10-22	378	2016-01-19	81	2016-12-17	97

Table A.2: List of extratropical storms constituting the historical data set.

Thunderstorms							
Date	**Outages**	**Date**	**Outages**	**Date**	**Outages**	**Date**	**Outages**
2005-06-28	423	2007-07-29	269	2009-07-29	347	2016-06-05	134
2005-07-18	606	2007-08-17	301	2009-08-21	622	2016-06-11	336
2005-07-21	279	2008-06-08	818	2010-05-03	483	2016-06-21	136
2005-07-27	859	2008-06-13	531	2010-06-02	253	2016-06-28	113
2005-08-04	490	2008-07-17	380	2013-05-29	361	2016-07-01	183
2005-09-16	340	2008-07-22	768	2013-09-01	212	2016-07-10	92
2005-10-07	662	2008-07-26	384	2014-05-27	269	2016-07-14	144
2006-07-27	1042	2008-08-07	258	2014-07-03	656	2016-08-10	649
2006-08-01	549	2008-09-06	669	2014-08-12	282	2016-08-12	555
2007-05-31	382	2009-07-06	438	2014-09-06	213	2016-08-14	342
2007-07-14	254	2009-07-23	358	2015-09-13	125	2016-08-16	138

Table A.3: List of thunderstorms constituting the historical data set.

Snow and ice storms					
Date	**Outages**	**Date**	**Outages**	**Date**	**Outages**
2005-12-16	131	2011-02-02	199	2016-04-03	740
2006-01-02	549	2011-10-29	25019	2016-12-17	107
2006-01-14	1560	2012-11-07	800	2017-01-23	723
2007-03-02	250	2012-12-28	132	2017-02-09	204
2007-12-02	467	2013-02-08	1097	2017-02-13	523
2008-01-13	652	2013-03-08	401	2017-03-10	71
2008-02-12	696	2014-02-05	33	2017-03-13	209
2008-12-10	615	2014-02-13	117	2017-12-09	81
2008-12-16	57	2014-11-26	507	2017-12-23	138
2008-12-30	454	2015-01-18	51	2018-01-04	164
2009-01-07	896	2015-01-26	46	2018-01-16	42
2009-01-10	34	2015-02-15	86	2018-01-30	37
2009-01-28	77	2016-01-12	84	2018-02-01	80
2010-02-23	163	2016-01-17	68	2018-02-07	70
2010-12-26	857	2016-01-23	42	2018-02-17	200
2011-01-12	152	2016-02-04	1663	2018-02-22	49
2011-01-18	444	2016-02-13	145	2018-03-07	5841
2011-01-26	108	2016-03-20	32	2018-03-13	577

Table A.4: List of snow and ice storms constituting the historical data set.

Bibliography

[1] D. Cerrai, D. W. Wanik, M. A. E. Bhuiyan, X. Zhang, J. Yang, M. E. Frediani, and E. N. Anagnostou, "Predicting storm outages through new representations of weather and vegetation," *IEEE Access*, vol. 7, pp. 29 639–29 654, 2019.

[2] J. McGee, J. Skiff, P. Carozza, T. Edelstein, L. Hoffman, S. Jackson, R. McGrath, F. McGroarty, and C. Osten, "Report of the two storm panel," *State of Connecticut*, 2012.

[3] C. Light and Power, "Transmission and distribution reliability performance 608 report," Tech. Rep., 2014.

[4] E. N. Lorenz, "Deterministic nonperiodic flow," *Journal of the atmospheric sciences*, vol. 20, no. 2, pp. 130–141, 1963.

[5] D. W. Wanik, E. N. Anagnostou, B. M. Hartman, M. E. B. Frediani, and M. Astitha, "Storm outage modeling for an electric distribution network in northeastern USA," *Natural Hazards*, vol. 79, no. 2, pp. 1359–1384, 2015.

[6] J. He, D. W. Wanik, B. M. Hartman, E. N. Anagnostou, M. Astitha, and M. E. B. Frediani, "Nonparametric tree-based predictive modeling of storm outages on an electric distribution network," *Risk Analysis*, vol. 37, no. 3, pp. 441–458, 2017.

[7] D. A. Jones, "Electrical engineering: the backbone of society," *IEEE Proceedings A - Science, Measurement and Technology*, vol. 138, no. 1, pp. 1–10, 1991.

[8] P. Schavemaker and L. V. der Sluis, *Electrical power system essentials*. John Wiley & Sons., 2008.

[9] M. Munasinghe and A. Sanghvi, "Reliability of electricity supply, outage costs and value of service: an overview," *The Energy Journal*, vol. 9, no. Special Issue 2, pp. 1–18, 1988.

[10] M. Schmidthaler and J. Reichl, "Assessing the socio-economic effects of power outages ad hoc," *Computer Science-Research and Development*, vol. 31, no. 3, pp. 157–161, 2016.

[11] I. Sanchez, "Short-term prediction of wind energy production," *International Journal of Forecasting*, vol. 22, no. 1, pp. 43–56, 2006.

[12] M. Zamo, O. Mestre, P. Arbogast, and O. Pannekoucke, "A benchmark of statistical regression methods for short-term forecasting of photovoltaic electricity production, part i: Deterministic forecast of hourly production," *Solar Energy*, vol. 105, pp. 792–803, 2014.

[13] C. Wan, Z. Xu, P. Pinson, Z. Y. Dong, and K. P. Wong, "Probabilistic forecasting of wind power generation using extreme learning machine," *IEEE Transactions on Power Systems*, vol. 29, no. 3, pp. 1033–1044, 2014.

[14] J. W. Taylor, "Short-term electricity demand forecasting using double seasonal exponential smoothing," *Journal of the Operational Research Society*, vol. 54, no. 8, pp. 799–805, 2003.

[15] J. W. Taylor, L. M. De Menezes, and P. E. McSharry, "A comparison of univariate methods for forecasting electricity demand up to a day ahead," *International Journal of Forecasting*, vol. 22, no. 1, pp. 1–16, 2006.

[16] T. Hong, P. Wang, and L. White, "Weather station selection for electric load forecasting," *International Journal of Forecasting*, vol. 31, no. 2, pp. 286–295, 2015.

[17] T. Hong and S. Fan, "Probabilistic electric load forecasting: A tutorial review," *International Journal of Forecasting*, vol. 32, no. 3, pp. 914–938, 2016.

[18] H. Liu, R. A. Davidson, D. V. Rosowsky, and J. R. Stedinger, "Negative binomial regression of electric power outages in hurricanes," *Journal of infrastructure systems*, vol. 11, no. 4, pp. 258–267, 2005.

[19] D. Wanik, E. Anagnostou, M. Astitha, B. Hartman, G. Lackmann, J. Yang, D. Cerrai, J. He, and M. Frediani, "A case study on power outage impacts from future hurricane sandy scenarios," *Journal of Applied Meteorology and Climatology*, vol. 57, no. 1, pp. 51–79, 2018.

[20] D. Chapman, "The cost of poor power quality," *Power Quality Aplication Guide*, pp. 1–4, 2001.

[21] C. Klinger and V. M. Owen Landeg, "Power outages, extreme events and health: a systematic review of the literature from 2011-2012," *PLoS currents*, vol. 6, 2014.

[22] G. B. Anderson and M. L. Bell, "Lights out: impact of the august 2003 power outage on mortality in new york, NY," *Epidemiology (Cambridge, Mass.)*, vol. 23, no. 2, p. 189, 2012.

[23] D. T. Ton and W. P. Wang, "A more resilient grid: The us department of energy joins with stakeholders in an R&D plan," *IEEE Power and Energy Magazine*, vol. 13, no. 3, pp. 26–34, 2015.

[24] R. K. Pachauri, M. R. Allen, V. R. Barros, J. Broome, W. Cramer, R. Christ, J. A. Church, L. Clarke, Q. Dahe, P. Dasgupta *et al.*, *Climate change 2014: synthesis report. Contribution of Working Groups I, II and III to the fifth assessment report of the Intergovernmental Panel on Climate Change*. IPCC, 2014.

[25] R. J. Campbell, "Weather-related power outages and electric system resiliency," Congressional Research Service, Library of Congress Washington, DC, 2012.

[26] D. Lubkeman and D. E. Julian, "Large scale storm outage management," in *Power Engineering Society General Meeting, 2004. IEEE.* IEEE, 2004, pp. 16–22.

[27] A. C. Cameron and P. K. Trivedi, *Regression analysis of count data*. Cambridge university press, 1998, vol. 30.

[28] H. Liu, R. A. Davidson, and T. V. Apanasovich, "Spatial generalized linear mixed models of electric power outages due to hurricanes and ice storms," *Reliability Engineering & System Safety*, vol. 93, no. 6, pp. 897–912, 2008.

[29] S.-R. Han, S. D. Guikema, S. M. Quiring, K.-H. Lee, D. Rosowsky, and R. A. Davidson, "Estimating the spatial distribution of power outages during hurricanes in the gulf coast region," *Reliability Engineering & System Safety*, vol. 94, no. 2, pp. 199–210, 2009.

[30] T. Hastie and R. Tibshirani, *Generalized additive models*. Wiley Online Library, 1990.

[31] S.-R. Han, S. D. Guikema, and S. M. Quiring, "Improving the predictive accuracy of hurricane power outage forecasts using generalized additive models," *Risk analysis*, vol. 29, no. 10, pp. 1443–1453, 2009.

[32] L. Breiman, "Random forests," *Machine learning*, vol. 45, no. 1, pp. 5–32, 2001.

[33] R. Nateghi, S. Guikema, and S. M. Quiring, "Power outage estimation for tropical cyclones: Improved accuracy with simpler models," *Risk analysis*, vol. 34, no. 6, pp. 1069–1078, 2014.

[34] S. D. Guikema and S. M. Quiring, "Hybrid data mining-regression for infrastructure risk assessment based on zero-inflated data," *Reliability Engineering & System Safety*, vol. 99, pp. 178–182, 2012.

[35] S. M. Quiring, A. B. Schumacher, and S. D. Guikema, "Incorporating hurricane forecast uncertainty into a decision-support application for power outage modeling," *Bulletin of the American Meteorological Society*, vol. 95, no. 1, pp. 47–58, 2014.

[36] L. Breiman, J. Friedman, C. J. Stone, and R. A. Olshen, *Classification and regression trees*. CRC press, 1984.

[37] D. B. McRoberts, S. M. Quiring, and S. D. Guikema, "Improving hurricane power outage prediction models through the inclusion of local environmental factors," *Risk analysis*, 2016.

[38] S. D. Guikema, R. Nateghi, S. M. Quiring, A. Staid, A. C. Reilly, and M. Gao, "Predicting hurricane power outages to support storm response planning," *IEEE Access*, vol. 2, pp. 1364–1373, 2014.

[39] D. Wanik, J. Parent, E. Anagnostou, and B. Hartman, "Using vegetation management and lidar-derived tree height data to improve outage predictions for electric utilities," *Electric Power Systems Research*, vol. 146, pp. 236–245, 2017.

[40] J. H. Friedman, "Greedy function approximation: a gradient boosting machine," *Annals of statistics*, pp. 1189–1232, 2001.

[41] H. A. Chipman, E. I. George, R. E. McCulloch *et al.*, "BART: Bayesian additive regression trees," *The Annals of Applied Statistics*, vol. 4, no. 1, pp. 266–298, 2010.

[42] N. Meinshausen, "Quantile regression forests," *Journal of Machine Learning Research*, vol. 7, no. Jun, pp. 983–999, 2006.

[43] M. S. Jones, B. A. Colle, and J. S. Tongue, "Evaluation of a mesoscale short-range ensemble forecast system over the northeast United States," *Weather and Forecasting*, vol. 22, no. 1, pp. 36–55, 2007.

[44] R. H. Langland, M. A. Shapiro, and R. Gelaro, "Initial condition sensitivity and error growth in forecasts of the 25 January 2000 East Coast snowstorm," *Monthly Weather Review*, vol. 130, no. 4, pp. 957–974, 2002.

[45] G. A. Grell, Y.-H. Kuo, and R. J. Pasch, "Semiprognostic tests of cumulus parameterization schemes in the middle latitudes," *Monthly weather review*, vol. 119, no. 1, pp. 5–31, 1991.

[46] M. E. Frediani, J. P. Hacker, E. N. Anagnostou, and T. Hopson, "Evaluation of PBL parameterizations for modeling surface wind speed during storms in the northeast united states," *Weather and Forecasting*, vol. 31, no. 5, pp. 1511–1528, 2016.

[47] G. Powers, X.-y. Huang, B. Klemp, C. Skamarock, J. Dudhia, O. Gill, G. Duda, D. Barker, and W. Wang, "A description of the advanced research WRF version 3," 2008.

[48] W. Wang, C. Bruyère, M. Duda, J. Dudhia, D. Gill, and H.-c. Lin, "ARW version 3 modelling system users guide," 2009.

[49] N. A. Phillips and J. Shukla, "On the strategy of combining coarse and fine grid meshes in numerical weather prediction," *Journal of Applied Meteorology*, vol. 12, no. 5, pp. 763–770, 1973.

[50] T. L. Clark and R. Farley, "Severe downslope windstorm calculations in two and three spatial dimensions using anelastic interactive grid nesting: A possible mechanism for gustiness," *Journal of the Atmospheric Sciences*, vol. 41, no. 3, pp. 329–350, 1984.

[51] D.-L. Zhang, H.-R. Chang, N. L. Seaman, T. T. Warner, and J. M. Fritsch, "A two-way interactive nesting procedure with variable terrain resolution," *Monthly Weather Review*, vol. 114, no. 7, pp. 1330–1339, 1986.

[52] G. Thompson, P. R. Field, R. M. Rasmussen, and W. D. Hall, "Explicit forecasts of winter precipitation using an improved bulk microphysics scheme. part ii: Implementation of a new snow parameterization," *Monthly Weather Review*, vol. 136, no. 12, pp. 5095–5115, 2008.

[53] G. A. Grell, "Prognostic evaluation of assumptions used by cumulus parameterizations," *Monthly Weather Review*, vol. 121, no. 3, pp. 764–787, 1993.

[54] G. A. Grell and D. Dévényi, "A generalized approach to parameterizing convection combining ensemble and data assimilation techniques," *Geophysical Research Letters*, vol. 29, no. 14, pp. 38–1, 2002.

[55] S.-Y. Hong, Y. Noh, and J. Dudhia, "A new vertical diffusion package with an explicit treatment of entrainment processes," *Monthly weather review*, vol. 134, no. 9, pp. 2318–2341, 2006.

[56] C. A. Paulson, "The mathematical representation of wind speed and temperature profiles in the unstable atmospheric surface layer," *Journal of Applied Meteorology*, vol. 9, no. 6, pp. 857–861, 1970.

[57] A. Dyer and B. Hicks, "Flux-gradient relationships in the constant flux layer," *Quarterly Journal of the Royal Meteorological Society*, vol. 96, no. 410, pp. 715–721, 1970.

[58] E. K. Webb, "Profile relationships: The log-linear range, and extension to strong stability," *Quarterly Journal of the Royal Meteorological Society*, vol. 96, no. 407, pp. 67–90, 1970.

[59] A. C. Beljaars, "The parametrization of surface fluxes in large-scale models under free convection," *Quarterly Journal of the Royal Meteorological Society*, vol. 121, no. 522, pp. 255–270, 1995.

[60] D. Zhang and R. A. Anthes, "A high-resolution model of the planetary boundary layersensitivity tests and comparisons with sesame-79 data," *Journal of Applied Meteorology*, vol. 21, no. 11, pp. 1594–1609, 1982.

[61] M. Tewari, F. Chen, W. Wang, J. Dudhia, M. LeMone, K. Mitchell, M. Ek, G. Gayno, J. Wegiel, and R. Cuenca, "Implementation and verification of the unified noah land surface model in the wrf model," in *20th conference on weather analysis and forecasting/16th conference on numerical weather prediction*, vol. 1115, 2004.

[62] E. J. Mlawer, S. J. Taubman, P. D. Brown, M. J. Iacono, and S. A. Clough, "Radiative transfer for inhomogeneous atmospheres: Rrtm, a validated correlated-k model for the longwave," *Journal of Geophysical Research: Atmospheres*, vol. 102, no. D14, pp. 16 663–16 682, 1997.

[63] M.-D. Chou, M. J. Suarez, X.-Z. Liang, M. M.-H. Yan, and C. Cote, "A thermal infrared radiation parameterization for atmospheric studies," 2001.

[64] M.-D. Chou and M. J. Suarez, "A solar radiation parameterization for atmospheric studies. volume 15," 1999.

[65] "Connecticut's changing landscape land cover," http://clear.uconn.edu/projects/landscape/, University of Connecticut, 2006, accessed: 2017-12-17.

[66] D. J. Watson, "Comparative physiological studies on the growth of field crops: I. variation in net assimilation rate and leaf area between species and varieties, and within and between years," *Annals of botany*, vol. 11, no. 41, pp. 41–76, 1947.

[67] "Leaf Area Index (1 Month - Terra/MODIS)," https://neo.sci.gsfc.nasa.gov/view.php?datasetId=MOD15A2_M_LAI, NASA Earth Observations, 2017, accessed: 2017-12-17.

[68] "NASA's Earth Observing System," https://eospso.nasa.gov/, NASA, 2017, accessed: 2017-12-17.

[69] A. L. Cauchy, "Sur l'équation à l'aide de laquelle on détermine les inégalités séculaires du mouvemeut des planètes." *O-euvres Complètes (IIème Série) (1829)*, 1829.

[70] K. Pearson, "LIII. On lines and planes of closest fit to systems of points in space," *The London, Edinburgh, and Dublin Philosophical Magazine and Journal of Science*, vol. 2, no. 11, pp. 559–572, 1901.

[71] H. F. Kaiser, "The varimax criterion for analytic rotation in factor analysis," *Psychometrika*, vol. 23, no. 3, pp. 187–200, 1958.

[72] D. T. Larose and C. D. Larose, *Data mining and predictive analytics*. John Wiley & Sons, 2015.

[73] T. Hastie, R. Tibshirani *et al.*, "Bayesian backfitting (with comments and a rejoinder by the authors," *Statistical Science*, vol. 15, no. 3, pp. 196–223, 2000.

[74] D. Wanik, E. Anagnostou, B. Hartman, and T. Layton, "Estimated time of restoration (etr) guidance for electric distribution networks," *Journal of Homeland Security and Emergency Management*, 2018.

[75] T. Walsh, T. Layton, D. Wanik, and J. Mellor, "Agent based model to estimate time to restoration of storm-induced power outages," *Infrastructures*, vol. 3, no. 3, p. 33, 2018.

[76] J. M. Wallace and P. V. Hobbs, *Atmospheric science: an introductory survey*. Academic press, 2006, vol. 92.

[77] "Severe weather 101," http://www.nssl.noaa.gov/education/svrwx101/, National Severe Storms Laboratory, 2017, accessed: 2017-12-17.

[78] J. E. Nash and J. V. Sutcliffe, "River flow forecasting through conceptual models part IA discussion of principles," *Journal of hydrology*, vol. 10, no. 3, pp. 282–290, 1970.

[79] D. R. Legates and G. J. McCabe, "Evaluating the use of goodness-of-fit measures in hydrologic and hydroclimatic model validation," *Water resources research*, vol. 35, no. 1, pp. 233–241, 1999.

[80] M. Stone, "Cross-validatory choice and assessment of statistical predictions," *Journal of the royal statistical society. Series B (Methodological)*, pp. 111–147, 1974.

[81] D. M. Allen, "The relationship between variable selection and data agumentation and a method for prediction," *Technometrics*, vol. 16, no. 1, pp. 125–127, 1974.

[82] S. Geisser, "The predictive sample reuse method with applications," *Journal of the American statistical Association*, vol. 70, no. 350, pp. 320–328, 1975.

[83] J. Han, J. Pei, and M. Kamber, *Data mining: concepts and techniques*. Elsevier, 2011.

[84] K. E. Taylor, "Summarizing multiple aspects of model performance in a single diagram," *Journal of Geophysical Research: Atmospheres*, vol. 106, no. D7, pp. 7183–7192, 2001.

[85] A. Rossa, P. Nurmi, and E. Ebert, "Overview of methods for the verification of quantitative precipitation forecasts," 2008.

[86] E. Ebert and J. McBride, "Verification of precipitation in weather systems: Determination of systematic errors," *Journal of Hydrology*, vol. 239, no. 1, pp. 179–202, 2000.

[87] J. Zepeda-Arce, E. Foufoula-Georgiou, and K. K. Droegemeier, "Space-time rainfall organization and its role in validating quantitative precipitation forecasts," *Journal of Geophysical Research: Atmospheres*, vol. 105, no. D8, pp. 10 129–10 146, 2000.

[88] T. Cherubini, A. Ghelli, and F. Lalaurette, "Verification of precipitation forecasts over the alpine region using a high-density observing network," *Weather and Forecasting*, vol. 17, no. 2, pp. 238–249, 2002.

[89] E. Yates, S. Anquetin, V. Ducrocq, J.-D. Creutin, D. Ricard, and K. Chancibault, "Point and areal validation of forecast precipitation fields," *Meteorological Applications*, vol. 13, no. 1, pp. 1–20, 2006.

[90] ISO, "12494:2017: Atmospheric icing of structures," International Organization for Standardization, Tech. Rep. ISO/TC 98/SC 3, 2017.

[91] M. Farzaneh, *Atmospheric icing of power networks*. Springer Science & Business Media, 2008.

[92] W. B. Bendel and D. Paton, "A review of the effect of ice storms on the power industry," *Journal of Applied Meteorology*, vol. 20, no. 12, pp. 1445–1449, 1981.

[93] E. L. Lecomte, A. W. Pang, and J. W. Russell, *Ice storm'98*. Institute for Catastrophic Loss Reduction Ottawa,, Canada, 1998.

[94] S. E. Chang, T. L. McDaniels, J. Mikawoz, and K. Peterson, "Infrastructure failure interdependencies in extreme events: power outage consequences in the 1998 ice storm," *Natural Hazards*, vol. 41, no. 2, pp. 337–358, 2007.

[95] J. Broder, A. Mehrotra, and J. Tintinalli, "Injuries from the 2002 north carolina ice storm, and strategies for prevention," *Injury*, vol. 36, no. 1, pp. 21–26, 2005.

[96] M. T. Rahman and T. Rashed, "Urban tree damage estimation using airborne laser scanner data and geographic information systems: An example from 2007 oklahoma ice storm," *Urban Forestry & Urban Greening*, vol. 14, no. 3, pp. 562–572, 2015.

[97] Z.-l. Jiang, J.-z. Lu, H.-c. Lei, and F.-y. HUANG, "Analysis of the causes of tower collapses in hunan during the 2008 ice storm," *High Voltage Engineering*, vol. 34, no. 11, pp. 2468–2474, 2008.

[98] B. Zhou, L. Gu, Y. Ding, L. Shao, Z. Wu, X. Yang, C. Li, Z. Li, X. Wang, Y. Cao *et al.*, "The great 2008 chinese ice storm: its socioeconomic–ecological impact and sustainability lessons learned," *Bulletin of the American Meteorological Society*, vol. 92, no. 1, pp. 47–60, 2011.

[99] L. Makkonen and B. Wichura, "Simulating wet snow loads on power line cables by a simple model," *Cold Regions Science and Technology*, vol. 61, no. 2-3, pp. 73–81, 2010.

[100] C. Klinger, M. Mehdianpour, D. Klingbeil, D. Bettge, R. Häcker, and W. Baer, "Failure analysis on collapsed towers of overhead electrical lines in the region münsterland (germany) 2005," *Engineering Failure Analysis*, vol. 18, no. 7, pp. 1873–1883, 2011.

[101] M. Llasat, M. Turco, P. Quintana-Seguí, and M. Llasat-Botija, "The snow storm of 8 march 2010 in catalonia (spain): a paradigmatic wet-snow event with a high societal impact," *Natural Hazards and Earth System Sciences*, vol. 14, no. 2, p. 427, 2014.

[102] D. LeComte, "Us weather highlights 2011: Unparalleled weather extremes," *Weatherwise*, vol. 65, no. 3, pp. 20–27, 2012.

[103] P. Kocin, "Some thoughts on the societal and economic impacts of winter storms," in *Workshop of the Social and Economic Impacts of Weather*. National Center for Atmospheric Research, 1997, pp. 55–60.

[104] B. Rippey, J. B. Halverson, H. Angeloff, T. Fathauer, B. Moore, A. Prechtel, and R. Thoman, "Weatherwatch: September/october 2011," *Weatherwise*, vol. 65, no. 1, pp. 50–65, 2012.

[105] FERC and NERC, "Transmission facility outages during the northeast snowstorm of october 29-30, 2011," Federal Energy Regulatory Commission and the North American Electric Reliability Corporation, Tech. Rep., 2012.

[106] P. M. Houck and N. B. Hampson, "Epidemic carbon monoxide poisoning following a winter storm," *The Journal of emergency medicine*, vol. 15, no. 4, pp. 469–473, 1997.

[107] W. R. Daley, A. Smith, E. Paz-Argandona, J. Malilay, and M. McGeehin, "An outbreak of carbon monoxide poisoning after a major ice storm in maine," *The Journal of emergency medicine*, vol. 18, no. 1, pp. 87–93, 2000.

[108] C. for Disease Control, Prevention *et al.*, "Use of carbon monoxide alarms to prevent poisonings during a power outage–north carolina, december 2002," *MMWR: Morbidity and mortality weekly report*, vol. 53, no. 9, pp. 189–192, 2004.

[109] K. K. Johnson-Arbor, A. S. Quental, and D. Li, "A comparison of carbon monoxide exposures after snowstorms and power outages," *American journal of preventive medicine*, vol. 46, no. 5, pp. 481–486, 2014.

[110] M. Tomaszewski and G. Bartodziej, "Prevention of effects of overhead line failures caused by ice and snow adhesion and accretion," *Cold Regions Science and Technology*, vol. 65, no. 2, pp. 211–218, 2011.

[111] E. Larouche, J. Rouat, G. Bouchard, and M. Farzaneh, "Exploration of static and time dependent neural network technique for the prediction of ice accretion on overhead line conductors," in *9th International Workshop on Atmospheric Icing of Structures. Chester, United Kingdom, Session*, vol. 2, 2000.

[112] A. Zarnani, P. Musilek, X. Shi, X. Ke, H. He, and R. Greiner, "Learning to predict ice accretion on electric power lines," *Engineering Applications of Artificial Intelligence*, vol. 25, no. 3, pp. 609–617, 2012.

[113] I. Imai, "Studies of ice accretion," *Res. Snow Ice*, vol. 1, pp. 35–44, 1953.

[114] R. W. Lenhard Jr, "An indirect method for estimating the weight of glaze on wires," *Bulletin of the American Meteorological Society*, vol. 36, no. 1, pp. 1–5, 1955.

[115] K. F. Jones, "A simple model for freezing rain ice loads," *Atmospheric research*, vol. 46, no. 1-2, pp. 87–97, 1998.

[116] P. M. Chaîné and G. Castonguay, *New approach to radial ice thickness concept applied to bundle-like conductors*. Environment Canada, Atmospheric Environment, 1974, vol. 4.

[117] E. J. Goodwin III, J. D. Mozer, A. DiGioia Jr, and B. Power, "Predicting ice and snow loads for transmission line design," PENNSYLVANIA POWER AND LIGHT CO ALLENTOWN PA, Tech. Rep., 1983.

[118] E. Lozowski, J. Stallabrass, and P. Hearty, "The icing of an unheated, nonrotating cylinder. part i: A simulation model," *Journal of climate and applied meteorology*, vol. 22, no. 12, pp. 2053–2062, 1983.

[119] L. Makkonen, "Modeling of ice accretion on wires," *Journal of climate and applied meteorology*, vol. 23, no. 6, pp. 929–939, 1984.

[120] ——, "Modeling power line icing in freezing precipitation," *Atmospheric research*, vol. 46, no. 1-2, pp. 131–142, 1998.

[121] Y. Sakamoto, "Snow accretion on overhead wires," *Philosophical Transactions of the Royal Society of London. Series A: Mathematical, Physical and Engineering Sciences*, vol. 358, no. 1776, pp. 2941–2970, 2000.

[122] L. Makkonen, "Estimation of wet snow accretion on structures," *Cold Regions Science and Technology*, vol. 17, no. 1, pp. 83–88, 1989.

[123] B. E. Kringlebotn Nygaard, H. Ágústsson, and K. Somfalvi-Tóth, "Modeling wet snow accretion on power lines: improvements to previous methods using 50 years of observations," *Journal of Applied Meteorology and Climatology*, vol. 52, no. 10, pp. 2189–2203, 2013.

[124] P. Admirat, "Wet snow accretion on overhead lines," in *Atmospheric Icing of Power Networks*. Springer, 2008, pp. 119–169.

[125] S. Haykin, *Neural networks*. Prentice hall New York, 1994, vol. 2.

[126] P. McComber, J. Druez, J. De Lafontaine, A. Paradis, J. Laflamme *et al.*, "Estimation of transmission line icing at different sites using a neural network," in *The Ninth International Offshore and Polar Engineering Conference*. International Society of Offshore and Polar Engineers, 1999.

[127] V. Vapnik, *The nature of statistical learning theory*. Springer science & business media, 2013.

[128] P. McCullagh, *Generalized linear models*. Routledge, 2018.

[129] P. Bourgouin, "A method to determine precipitation types," *Weather and Forecasting*, vol. 15, no. 5, pp. 583–592, 2000.

[130] G. S. Manikin, K. F. Brill, and B. Ferrier, "An eta model precipitation type mini-ensemble for winter weather forecasting," in *16th Conf on Numerical Weather Prediction, Amer. Meteor. Soc., Seattle, WA, paper*, vol. 23, 2004.

[131] S. Geoffrey, "An overview of precipitation type forecasting using nam and sref data," in *21st Conference on Weather Analysis and Forecasting/17th Conference on Numerical Weather Prediction*, 2005.

[132] U. Gjertsen and V. Ødegaard, "The water phase of precipitationa comparison between observed, estimated and predicted values," *Atmospheric Research*, vol. 77, no. 1-4, pp. 218–231, 2005.

[133] M. S. Wandishin, M. E. Baldwin, S. L. Mullen, and J. V. Cortinas Jr, "Short-range ensemble forecasts of precipitation type," *Weather and Forecasting*, vol. 20, no. 4, pp. 609–626, 2005.

[134] K. Ikeda, M. Steiner, J. Pinto, and C. Alexander, "Evaluation of cold-season precipitation forecasts generated by the hourly updating high-resolution rapid refresh model," *Weather and Forecasting*, vol. 28, no. 4, pp. 921–939, 2013.

[135] H. D. Reeves, K. L. Elmore, A. Ryzhkov, T. Schuur, and J. Krause, "Sources of uncertainty in precipitation-type forecasting," *Weather and Forecasting*, vol. 29, no. 4, pp. 936–953, 2014.

[136] K. L. Elmore, H. M. Grams, D. Apps, and H. D. Reeves, "Verifying forecast precipitation type with mping," *Weather and Forecasting*, vol. 30, no. 3, pp. 656–667, 2015.

[137] H. D. Reeves, "The uncertainty of precipitation-type observations and its effect on the validation of forecast precipitation type," *Weather and Forecasting*, vol. 31, no. 6, pp. 1961–1971, 2016.

[138] NCEP and NOAA, "NCEP north american mesoscale (NAM) 12 km analysis," Boulder CO, 2015. [Online]. Available: http://rda.ucar.edu/datasets/ds609.0/

[139] G. Creighton, E. Kuchera, R. Adams-Selin, J. McCormick, S. Rentschler, and B. Wickard, "Afwa diagnostics in wrf," 2014.

[140] M. J. Iacono, J. S. Delamere, E. J. Mlawer, M. W. Shephard, S. A. Clough, and W. D. Collins, "Radiative forcing by long-lived greenhouse gases: Calculations with the aer radiative transfer models," *Journal of Geophysical Research: Atmospheres*, vol. 113, no. D13, 2008.

[141] C. Homer, J. Dewitz, L. Yang, S. Jin, P. Danielson, G. Xian, J. Coulston, N. Herold, J. Wickham, and K. Megown, "Completion of the 2011 national land cover database for the conterminous united states–representing a decade of land cover change information," *Photogrammetric Engineering & Remote Sensing*, vol. 81, no. 5, pp. 345–354, 2015.

[142] D. Gesch, G. Evans, M. Oimoen, and S. Arundel, "The national elevation dataset," American Society for Photogrammetry and Remote Sensing, Tech. Rep. 83-110, 2018.

[143] U. S. D. of Agriculture, "Soil survey geographic database (ssurgo)," 2018.

[144] P. J. Roebber, S. L. Bruening, D. M. Schultz, and J. V. Cortinas Jr, "Improving snowfall forecasting by diagnosing snow density," *Weather and forecasting*, vol. 18, no. 2, pp. 264–287, 2003.

[145] J. Weng, L. Liu, and J. Rong, "Impacts of snowy weather conditions on expressway traffic flow characteristics," *Discrete dynamics in nature and society*, vol. 2013, 2013.

[146] K. J. Sanders and B. L. Barjenbruch, "Analysis of ice-to-liquid ratios during freezing rain and the development of an ice accumulation model," *Weather and Forecasting*, vol. 31, no. 4, pp. 1041–1060, 2016.

[147] G. D. McManus, S. Piltz, S. Sperry, R. McPherson, A. Gartside, D. McClain, T. Meyer, C. Fetsch, and M. Shafer, "Development and testing of an ice accumulation algorithm." [Online]. Available: http://citeseerx.ist.psu.edu/viewdoc/download?doi=10.1.1.523.1125&rep=rep1&type=pdf

[148] P. McCullagh, *Generalized linear models*. Chapman and Hall/CRC, 1989.

[149] A. J. Dobson and A. Barnett, *An introduction to generalized linear models*. Chapman and Hall/CRC, 2008.

[150] R. H. Yahner and R. J. Hutnik, "Integrated vegetation management on an electric transmission right-of-way in southeastern pennsylvania, us," *Journal of arboriculture*, 2005.

[151] P. A. Kuntz, R. D. Christie, and S. S. Venkata, "Optimal vegetation maintenance scheduling of overhead electric power distribution systems," *IEEE Transactions on Power Delivery*, vol. 17, no. 4, pp. 1164–1169, 2002.

[152] P. Simpson and R. Van Bossuyt, "Tree-caused electric outages," *Journal of Arboriculture*, vol. 22, pp. 117–121, 1996.

[153] D. T. Radmer, P. A. Kuntz, R. D. Christie, S. S. Venkata, and R. H. Fletcher, "Predicting vegetation-related failure rates for overhead distribution feeders," *IEEE Transactions on Power Delivery*, vol. 17, no. 4, pp. 1170–1175, 2002.

[154] F. E. R. Commission *et al.*, "Utility vegetation management final report. march 2004," *Link.(commissioned to support the investigation of the 2003 Northeast blackout.)*.

[155] P. J. Appelt and J. W. Goodfellow, "Research on how trees cause interruptions-applications to vegetation management," in *Rural Electric Power Conference, 2004.* IEEE, 2004, pp. C6–1.

[156] W. House, "Economic benefits of increasing electric grid resilience to weather outages," *Washington, DC: Executive Office of the President*, 2013.

[157] G. Paula, "Right-of-way maintenance: Changing options," *Elect. World T&D Special Rep*, vol. 203, no. 9, pp. S5–S15, 1989.

[158] W. Lovelace, "Vegetation management on distribution line right-of-way are you getting top value for your money?" in *Rural Electric Power Conference, 1996. Papers Presented at the 39th Annual Conference.* IEEE, 1996, p. B5.

[159] "Understanding vegetation management," https://www.eversource.com/content/docs/default-source/nh---pdfs/eversource-veg-mgmt-guide_final_web.pdf, University of Connecticut, 2018, accessed: 2018-04-10.

[160] T. R. Oke, "The micrometeorology of the urban forest," *Philosophical Transactions of the Royal Society of London. B, Biological Sciences*, vol. 324, no. 1223, pp. 335–349, 1989.

[161] N. J. Georgi and K. Zafiriadis, "The impact of park trees on microclimate in urban areas," *Urban Ecosystems*, vol. 9, no. 3, pp. 195–209, 2006.

[162] E. G. McPherson, D. J. Nowak, and R. A. Rowntree, *Chicago's urban forest ecosystem: results of the Chicago Urban Forest Climate Project.* US Department of Agriculture, Forest Service, Northeastern Forest Experiment , 1994, vol. 186.

[163] D. J. Nowak *et al.*, "The effects of urban trees on air quality," *USDA Forest Service*, pp. 96–102, 2002.

[164] D. J. Nowak, D. E. Crane, and J. C. Stevens, "Air pollution removal by urban trees and shrubs in the united states," *Urban forestry & urban greening*, vol. 4, no. 3-4, pp. 115–123, 2006.

[165] J. Yang, J. McBride, J. Zhou, and Z. Sun, "The urban forest in beijing and its role in air pollution reduction," *Urban forestry & urban greening*, vol. 3, no. 2, pp. 65–78, 2005.

[166] J. F. Dwyer, E. G. McPherson, H. W. Schroeder, and R. A. Rowntree, "Assessing the benefits and costs of the urban forest," *Journal of Arboriculture*, vol. 18, pp. 227–227, 1992.

[167] D. J. Nowak and J. F. Dwyer, "Understanding the benefits and costs of urban forest ecosystems," in *Urban and community forestry in the northeast.* Springer, 2007, pp. 25–46.

[168] W. B. Most and S. Weissman, "Trees and power lines: minimizing conflicts between electric power infrastructure and the urban forest," 2012.

[169] "Pura calls for suspension of enhanced tree trimming," https://www.ct.gov/pura/cwp/view.asp?Q=541516, Public Utilities Regulatory Agency, Department of Energy & Environmental Protection, 2014, accessed: 2019-04-03.

[170] S. D. Guikema, R. A. Davidson, and H. Liu, "Statistical models of the effects of tree trimming on power system outages," *IEEE Transactions on Power Delivery*, vol. 21, no. 3, pp. 1549–1557, 2006.

[171] "National land cover database," https://www.mrlc.gov/, MRLC, 2018, accessed: 2018-07-01.

[172] V. V. Salomonson, W. Barnes, P. W. Maymon, H. E. Montgomery, and H. Ostrow, "Modis: Advanced facility instrument for studies of the earth as a system," *IEEE Transactions on Geoscience and Remote Sensing*, vol. 27, no. 2, pp. 145–153, 1989.

[173] E. B. Wilson, "Probable inference, the law of succession, and statistical inference," *Journal of the American Statistical Association*, vol. 22, no. 158, pp. 209–212, 1927.

[174] R. G. Newcombe, "Two-sided confidence intervals for the single proportion: comparison of seven methods," *Statistics in medicine*, vol. 17, no. 8, pp. 857–872, 1998.

[175] T. Strutz, *Data fitting and uncertainty: A practical introduction to weighted least squares and beyond*. Vieweg and Teubner, 2010.

[176] C. C. Clogg, E. Petkova, and A. Haritou, "Statistical methods for comparing regression coefficients between models," *American Journal of Sociology*, vol. 100, no. 5, pp. 1261–1293, 1995.

[177] R. Paternoster, R. Brame, P. Mazerolle, and A. Piquero, "Using the correct statistical test for the equality of regression coefficients," *Criminology*, vol. 36, no. 4, pp. 859–866, 1998.

[178] Student, "The probable error of a mean," *Biometrika*, pp. 1–25, 1908.

[179] J. L. Fleiss, B. Levin, and M. C. Paik, *Statistical methods for rates and proportions*. John Wiley & Sons, 2013.